Aggregation-induced emission: phenomenon, mechanism and applications

Yuning Hong,[a] Jacky W. Y. Lam[a] and Ben Zhong Tang*[ab]

Received (in Cambridge, UK) 6th March 2009, Accepted 21st April 2009
First published as an Advance Article on the web 13th May 2009
DOI: 10.1039/b904665h

It is textbook knowledge that chromophore aggregation generally quenches light emission. In this feature article, we give an account on how we observed an opposite phenomenon termed aggregation-induced emission (AIE) and identified the restriction of intramolecular rotation as a main cause for the AIE effect. Based on the mechanistic understanding, we developed a series of new fluorescent and phosphorescent AIE systems with emission colours covering the entire visible spectral region and luminescence quantum yields up to unity. We explored high-tech applications of the AIE luminogens as, for example, fluorescence sensors (for explosive, ion, pH, temperature, viscosity, pressure, *etc.*), biological probes (for protein, DNA, RNA, sugar, phospholipid, *etc.*), immunoassay markers, PAGE visualization agents, polarized light emitters, monitors for layer-by-layer assembly, reporters for micelle formation, multistimuli-responsive nanomaterials, and active layers in the fabrication of organic light-emitting diodes.

Introduction

About half a century ago, Förster and Kasper discovered that the fluorescence of pyrene was weakened with an increase in its solution concentration.[1] It was soon recognized that this was a general phenomenon for many aromatic compounds.[2,3] This concentration-quenching effect was found to be caused by the formation of sandwich-shaped excimers and exciplexes aided by the collisional interactions between the aromatic molecules in the excited and ground states, which "are now known to be common to most aromatic hydrocarbons and their derivatives", as summarized by Birks in his classic book on *Photophysics of Aromatic Molecules* in 1970.[2]

The ubiquitous concentration–quenching effect has forced researchers to study and utilize fluorophores as isolated single molecules in very dilute solutions.[4] The use of dilute solutions, however, causes many problems. For example, emissions from dilute solutions are often weak, leading to poor sensitivity in fluorescence sensory systems, especially in bioassays of trace amounts of biomolecules.[5] The sensitivity cannot be enhanced by using high fluorophore concentration due to the notorious concentration-quenching effect. The small numbers of the dye molecules in dilute solutions can be quickly photobleached when a harsh laser beam is used as the excitation light source. The development of inorganic quantum dots (QDs) can surmount these disadvantages but poses new problems, such as difficult synthesis, limited variety and high cytotoxicity.[6]

Even in dilute solutions, concentration-quenching can still be involved. For example, in a bioassay system, the small fluorophore molecules may accumulate on the surfaces of the biomacromolecules and cluster in the hydrophobic cavities or pockets of the folding structures.[7] This can greatly increase local fluorophore concentration and cause the concentration-quenching problem. The concentration-quenching effect has been a thorny obstacle to the development of biosensor strips for on-site detection because the fluorophore concentration reaches its highest value in the solid state.[4,5]

[a] *Department of Chemistry, Nano Science and Technology Program, Bioengineering Graduate Program, The Hong Kong University of Science & Technology (HKUST), Clear Water Bay, Kowloon, Hong Kong, China. E-mail: tangbenz@ust.hk*
[b] *Department of Polymer Science & Engineering, Institute of Biomedical Macromolecules, Zhejiang University, Hangzhou 310027, China*

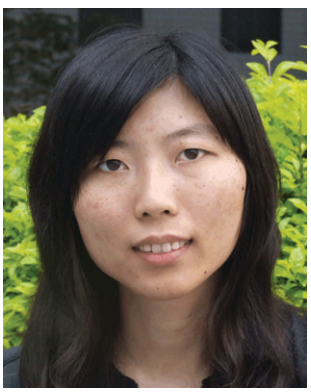

Yuning Hong

Yuning Hong received her BSc degree in applied chemistry from Sun Yat-sen University in 2006. She is now a PhD student in the Tang group at HKUST. Her interest is mainly in the development of new AIE molecules and exploration of their biological applications.

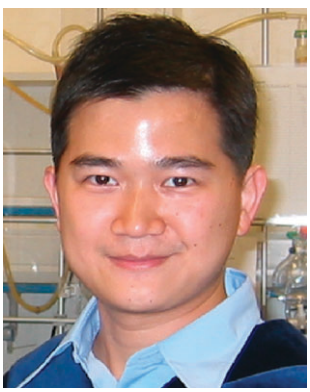

Jacky W. Y. Lam

Jacky W. Y. Lam received his PhD degree from HKUST in 2003 under the supervision of Prof. Tang. In 2003–2007, he did his postdoctoral work on novel polymers with linear and hyperbranched structures and advanced functional properties in the Tang group. He is currently a research assistant professor of chemistry at HKUST.

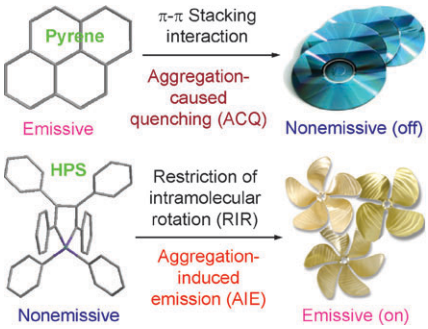

Chart 1 Planar luminogens such as pyrene tend to aggregate just as discs pile up due to strong π–π stacking interactions, which commonly turn "off" light emission, whereas nonplanar propeller-shaped luminogens such as hexaphenylsilole (HPS) behave oppositely, with their light emissions turned "on" by aggregate formation, due to the restricted intramolecular rotation in the aggregates.

Because there is no "solvent" in the solid state, the "solute" molecules are located in the immediate vicinity. The aromatic rings of the neighbouring fluorophores, especially those with disc-like shapes, experience strong π–π stacking interactions, which promotes the formation of aggregates with ordered or random structures. The excited states of the aggregates often decay *via* non-radiative pathways, which is notoriously known as aggregation-caused quenching (ACQ) of light emission in the condensed phase (Chart 1).[8]

The development of efficient luminescent materials is a topic of great current interest.[8,9] Whereas luminescence behaviours of *molecules* are normally investigated in the solution state, they are practically used as *materials* commonly in the solid state, for example, as thin films in the fabrication of organic light-emitting diodes (OLEDs)[9,10] and fluorescent diagnostic kits.[5,7] The ACQ effect, however, comes into play in the solid state, which has prevented many lead luminogens identified by the laboratory solution-screening process from finding real-world applications in an engineering robust form.

To mitigate the ACQ effect, various chemical, physical and engineering approaches and processes have been developed. For example, branched chains, bulky cyclics, spiro kinks, and dendritic wedges have been covalently attached to aromatic rings to obstruct the formation of aggregates.[11] Luminogens, especially red emitters with big fused polynuclear cores, have been physically passivated *via* surfactant encapsulation or doped into matrices of non-conjugated transparent polymers such as poly(methyl methacrylate) (PMMA).[12]

The chemical approaches, however, at times require painstaking synthetic effort, and the physical processes sometimes demand elaborate engineering control. The attachment of the non-conjugated groups to the aromatic rings is passive and can even be destructive. For example, the sterically bulky pendant groups can severely twist the conformations of the luminogens and thus disastrously jeopardize their π-electron conjugation. On the other hand, the non-conjugated encapsulants and the transparent matrices used in the physical processes are non-emissive and insulating and are hence dilutants and barriers for luminogen density and charge transport, respectively. The spatial distribution of the luminogen dopants in a doped film suffers from temporal instability: the luminogens dispersed in the polymer matrixes gradually migrate together over time, eventually forming large aggregates.

Although various approaches have been taken to interfere with luminogen aggregation, the attempts have met with only limited success. In many cases, aggregation was impeded only partially or temporarily.[11,12] The difficulty lies in the fact that aggregate formation is an intrinsic process when luminogenic molecules are located in close vicinity in the condensed phase. It will be nice, if a system can be developed, in which light emission is enhanced, rather than quenched, by aggregation. This will make life much easier because the aggregation now works to our benefit: no hard work will need to be done to artificially interrupt the very natural process of luminophore aggregation.[13,14]

In 2001, we discovered such a system, in which luminogen aggregation played a constructive, instead of a destructive, role in the light-emitting process: a series of silole molecules were found to be non-luminescent in the solution state but emissive in the aggregated state (as nanoparticle suspensions in poor solvents or as thin films in the solid state).[15] We coined the term "aggregation-induced emission" (AIE) for this novel phenomenon, because the non-luminescent silole molecules were induced to emit by aggregate formation.[15,16]

The novel AIE effect is exactly opposite to the notorious ACQ effect discussed above. The phenomenon is of academic value: whilst there are matured theories to explain the ACQ effect, new models will need to be established to understand the abnormal AIE effect. The phenomenon also has practical implications: in the AIE system, one can buoyantly enjoy the advantages of aggregate formation, rather than work against it. It will permit the use of dye solutions with any concentration for bioassays and enables the development of "turn on" or "light up" nanosensors by taking advantage of luminogenic aggregation.

The nanoaggregate-based AIE sensors are in some sense the organic versions of inorganic QD-based sensors. The QDs are commonly comprised of heavy metals and chalcogenic elements (*e.g.*, ZnSe, CdS, PdTe and CdSe/Te CdHgTe alloys) and are thus inherently cytotoxic. It is envisaged that the AIE

Ben Zhong Tang

Ben Zhong Tang received his PhD degree from Kyoto University and conducted his postdoctoral work at the University of Toronto. He joined HKUST in 1994 and was promoted to Chair Professor in 2008. He is interested in creating new molecules with novel structures and unique properties. He received a Natural Science Award from the Chinese Government and a Senior Research Fellowship from the Croucher Foundation in 2007. He serves as a science news contributor to Noteworthy Chemistry (ACS) and is a member of the editorial boards of a dozen scientific journals, including Macromolecules (ACS) and Progress in Polymer Science (Elsevier).

nanosensors will be as sensitive as, but much less cytotoxic than, their inorganic QD counterparts.[6]

Attracted by the intriguing phenomenon and its fascinating perspectives, we embarked on a program directed towards the decipherment of the working principle behind the AIE process, because a correct mechanistic understanding would help guide us to design new AIE luminogens and to explore their high-tech applications. In this feature article, we summarize what we have done in the area in the past years. We have identified restriction of intramolecular rotation (RIR) in the aggregates as a main cause for the AIE effect (Chart 1), developed a large variety of new AIE luminogens based on the RIR mechanism, and explored their utilities as functional materials, especially as chemosensors, bioprobes and solid-state emitters. We have succeeded in the creation of efficient phosphorescent systems based on simple organic crystals at room temperature, which is extremely rare, because it is well known that pure organic phosphorescence is inefficient under ambient conditions.[3]

Phenomenon

Our research group has been interested in alkyne chemistry and has employed acetylenic triple bonds as building blocks to construct new molecules and polymers with linear and hyperbranched structures and advanced functional properties.[17,18] In our search for efficient luminophores, we were attracted by a group of molecules called siloles, which were accessible by silylation of metallated alkynes.[15,19] A silole molecule named hexaphenylsilole (HPS or **1**) is shown in Fig. 1 as an example, whose electronic structure looks extensively conjugated. We intuitively thought that its solution should be highly emissive. However, we found with astonishment that it was not the case.

HPS: a special case

We prepared HPS by silylation of lithiated diphenylacetylene. Before purifying the reaction product by silica-gel column, we ran a routine thin-layer chromatography (TLC) test. When the TLC plate was taken out from the development tank, we were amazed that hardly any spots could be seen on the plate under illumination of a UV lamp. However, after the solvent was evaporated from the plate, a green light-emitting spot became visible. Thus, the fluorescence was off and on in the wet and dry plates, respectively, implying that the HPS molecules are non-luminescent when dissolved but become highly emissive when aggregated.[20] This extraordinary observation spurred us to further investigate its luminescence behaviour.

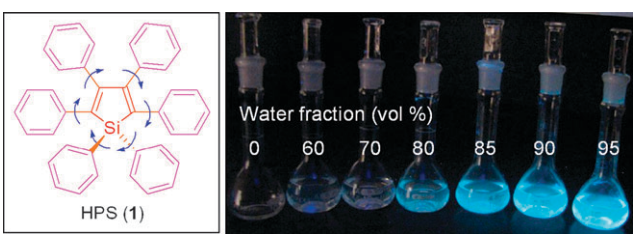

Fig. 1 (Left) Chemical structure of HPS. (Right) HPS solutions in acetonitrile–water mixtures containing different volume fractions of water; photographs taken under illumination of a UV lamp.

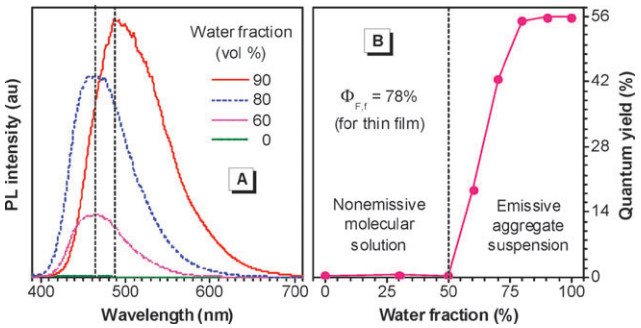

Fig. 2 (A) PL spectra of HPS solutions in acetonitrile–water mixtures. (B) Fluorescence quantum yield (Φ_F) of HPS *versus* solvent composition of the acetonitrile–water mixture. Data for a thin film of HPS ($\Phi_{F,f}$) are given in panel B for comparison. Reproduced with permission from ref. 20. Copyright (2003) American Chemical Society.

HPS is very soluble in acetonitrile, tetrahydrofuran (THF) and chloroform, slightly soluble in methanol, but completely insoluble in water. Solutions of HPS in its good solvents are non-emissive, as can be seen from the example shown in Fig. 1 for its solution in acetonitrile. Addition of large amounts of water into the acetonitrile solution of HPS causes the silole molecules to aggregate and induces them to emit efficiently. This duly substantiates the observation in the TLC test: HPS is induced to emit by aggregation. In other words, it is AIE active.

The intriguing AIE phenomenon was further confirmed by spectroscopic analyses. The photoluminescence (PL) spectrum of the HPS solution in acetonitrile is nearly a flat line parallel to the abscissa (Fig. 2A), with a fluorescence quantum yield (Φ_F) as low as 0.22%.[20] The Φ_F value remains unchanged until ~50% water is added into the solution. Afterwards, the Φ_F value increases swiftly (Fig. 2B). In the solvent mixture with 99% water, the Φ_F value of HPS rises to ~56%, which is ~255-fold higher than that in the pure acetonitrile solution. The AIE effect has enabled HPS to emit efficiently in the solid state: the emission efficiency of a thin film of HPS ($\Phi_{F,f}$) is as high as 78%, as estimated by employing a film of tris(8-hydroxyquinolinato)aluminium(III) (AlQ_3) as standard.[21]

Other silole derivatives: generalization

Is the AIE effect an isolated phenomenon for HPS alone or a general property for the silole family? To answer this question, we prepared a variety of silole derivatives and examined their photophysical properties in both solution and aggregate states. All the derivatives behave like HPS. For example, 1-methyl-pentaphenylsilole (MPPS; Chart 2) was non-luminescent when dissolved in good solvents (*e.g.*, Φ_F = 0.06% in ethanol)[15,20] but became very emissive when aggregated in poor solvents or fabricated into a thin film ($\Phi_{F,f}$ = 85%).[21] The aggregation boosted its emission efficiency by as much as 1417 times!

The silole derivatives share the following common features of photophysical behaviour: (1) In good solvents or aqueous mixtures with "low" water content (≤50%), they are non-emissive, with Φ_F values in the vicinity of 0.1%, (2) in solvent mixtures with "medium" water content, their emission progressively intensifies with increasing water content, and

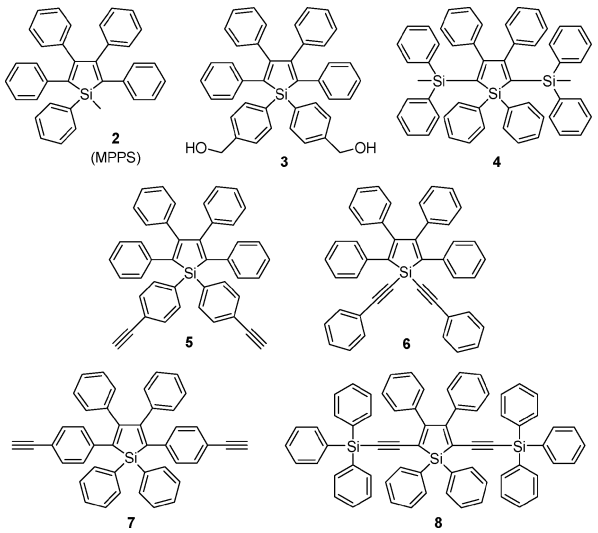

Chart 2 Examples of silole fluorogens prepared in our laboratories.

(3) in solvent mixtures with "high" water content (>80%), their PL spectra bathochromically shift.

In all the solvent mixtures, including those with high water contents, the silole derivatives give similar absorption spectra. Their spectral profiles experience little red shifts, as can be seen from the example shown in Fig. 3A for HPS solutions. The spectra of HPS measured in solvent mixtures with high water content show absorption tails extending well into the long wavelength region. This implies that the HPS molecules have aggregated into nanoparticles in the aqueous mixtures, because it is well known that the Mie effect of nanoparticles causes such level-off tails in the absorption spectra.[22]

Particle size analyses reveal the existence of particles with average sizes of 190 and 130 nm in the solvent mixtures with 80% and 90% water, respectively (Fig. 3), confirming that the HPS molecules have indeed aggregated into nanoparticles. In the solvent mixtures with water contents ≤50%, no level-off spectral tails in the long wavelength region are recorded by the UV-vis spectrometer and no nanoparticles are detected by the particle size analyzer, proving that the HPS molecules are genuinely dissolved as isolated species in the solvent mixtures with "low" water contents.

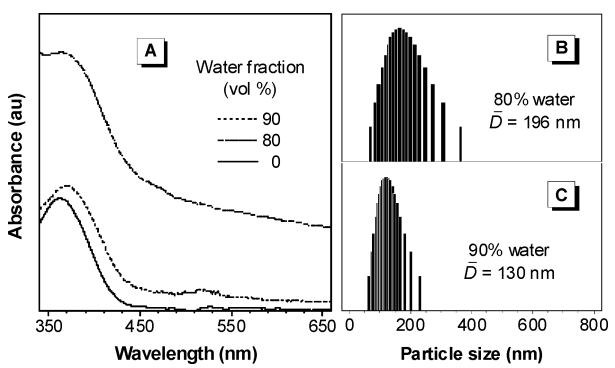

Fig. 3 (A) Absorption spectra of HPS in acetonitrile–water mixtures. Size distributions of nanoparticles of HPS in acetonitrile–water mixtures containing (B) 80% and (C) 90% water. Reproduced with permission from ref. 20. Copyright (2003) American Chemical Society.

Mechanism

It has become clear that the abnormal phenomenon of AIE is actually a general property for the silole family (Chart 2). The question we need to answer now is "what is the mechanistic cause for the AIE effect?" Deciphering its working principle may help gain new photophysical insights and spawn fresh technological innovations. We considered a number of possible mechanistic pathways, including conformational planarization, J-aggregate formation, and twisted intramolecular charge transfer (TICT), none of which, however, was fully supported by the experimental data.

If the conformation of HPS molecules became more planar upon aggregate formation, both absorption and emission spectra would bathochromically shift. The spectra of HPS, however, do not change much in the mixtures with different water contents (up to ~80%; Fig. 2 and 3). Crystal structure analysis reveals that the conformation of the HPS molecules remains twisted in the solid state.[20,21] These experimental observations exclude the possibility that the conformational planarization is a major cause of the AIE phenomenon.

The silole derivatives are basically nonpolar hydrophobic molecules. They contain no polar moieties such as donor (D) and acceptor (A) functional groups and hence experience no D–A or push–pull interactions. This structural feature makes it unlikely for the silole molecules to form J-aggregates, as verified by the X-ray diffraction (XRD) measurements.[20] This also rules out the possible involvement of the TICT process. If the TICT mechanism was at work, the spectra would red shift with an increase in solvent polarity. However, little change in the absorption spectra of HPS was observed when the solvent was changed from cyclohexane (λ_{ab} = 363 nm) to acetonitrile (λ_{ab} = 360 nm).[20]

Fundamental physics teaches us that any molecular motions consume energy. As can be seen from the left panel of Fig. 1, six phenyl peripheries are attached to one silole core in HPS; the former (rotors) can rotate against the latter (stator) *via* the single-bond axes. In the solutions, the intramolecular rotation is active, which serves as a relaxation channel for the excited state to decay. In the aggregates, the rotation is restricted due to the physical constraint, which blocks the non-radiative path and activates the radiative decay. We thus hypothesize that the RIR process is a cause for the AIE effect (Chart 1). To check the validity of this hypothesis, we performed a series of tests to externally and internally modulate the RIR process.

Viscochromism

As an external control, we first checked the effect of solvent viscosity on the silole emission. The RIR process is expected to be affected by the medium viscosity: the more viscous the medium, the slower the intramolecular rotation and hence the stronger the silole emission. Glycerol is a very viscous liquid, whose viscosity at 25 °C is about 1720-fold higher than that of methanol. Blending glycerol with methanol at different ratios can therefore afford solvent mixtures with drastically different viscosities.

As expected, the fluorescence of HPS is intensified with an increase in the viscosity of the solvent mixture (Fig. 4A).[20] In the mixtures with glycerol fractions of <50%, the PL intensity

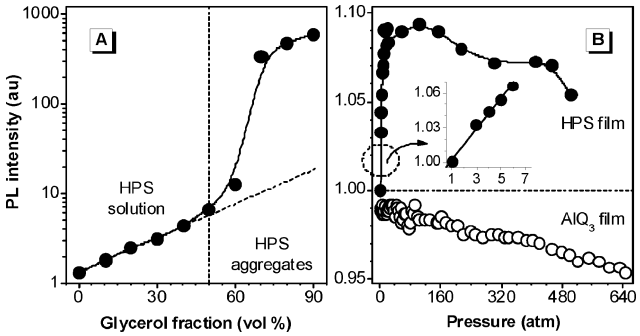

Fig. 4 Effects of (A) composition of glycerol–methanol mixture and (B) externally applied pressure on the PL intensity of HPS. Data for an AlQ_3 film is shown in panel B for comparison. The data given in panels A and B are reproduced with permission from ref. 20 [Copyright (2003) American Chemical Society] and 23 [Copyright (2008) The Royal Society of Chemistry], respectively.

increases "linearly" with viscosity on the semilog scale. The emission enhancement in this region should be predominantly due to the viscosity effect (viscochromism), because the silole molecules are soluble in these mixtures (*cf.*, Fig. 2B). In the mixtures with glycerol fractions of >50%, the PL intensity mounts rapidly, due to the aggregate formation caused by the poor solubility of the silole molecules in the mixtures with high glycerol content.

Piezochromism

We then investigated the effect of pressure on the emission of HPS. Pressurization exerts complex effects on the HPS luminescence.[23] The emission is first enhanced to a plateau at a very fast speed upon pressurization, showing a unique effect of pressurization-enhanced emission or piezochromism (Fig. 4B). However, when the HPS film is further pressurized, its emission slowly decreases from the plateau. Theoretically, pressurization imposes antagonistic effects on light emission. Pressurization brings molecules closer. The reduced distance between the dyes decreases the freedom of their molecular motion and strengthens the RIR process. On the other hand, it boosts molecular interactions and promotes excimer formation.[24] The RIR process enhances, but the excimer formation weakens, light emission.

The latter effect, *i.e.*, pressurization-caused quenching, has been commonly observed in conventional luminophore systems.[24] This is manifested by the result obtained from the control experiment on a solid film of AlQ_3: its PL intensity is monotonously weakened with increasing pressure (Fig. 4B).[23] This is probably due to pressurization-enhanced π–π stacking interactions between the plate-like quinoline rings. It is worth noting that the intramolecular rotation in an AlQ_3 molecule is prohibited because its quinoline rings are rigidly held together by the multiple bonds between the aromatic (quinoline) rings and the metal (aluminium) center.

The benzene rings in an HPS molecule, however, can rotate because its phenyl peripheries are linked to the silole core *via* single bonds. The steric effect between the phenyl rings forces the molecules to take a twisted propeller-shaped conformation, making it difficult for them to assume a dense packing structure when deposited onto the substrate by the vapor deposition process (*cf.*, Chart 1). In the molecular voids generated by loose packing, the HPS molecules can still undergo rotational motion to a limited extent. Pressurization decreases the void volumes and densifies the molecular packing. This strengthens the RIR process and therefore boosts the silole emission. Further pressurization, however, brings the silole molecules into such a close vicinity that excimer formation becomes possible. This may explain why the silole emission slowly drops from the plateau in the high pressure region.[23]

The molecular motion of HPS mainly consists of rotation (*e.g.*, C_{Ph}–C_{silole} torsion) and vibration (*e.g.*, C_{Ph}–C_{silole} stretch and bending). The change in the solvent viscosity can hardly affect the vibrational motion.[20] The pressurization in the low pressure region can shorten the distance between, but exert little effect on the distance within, the silole molecules.[24] The piezochromism observed in the low pressure region should be caused mainly by the suppression of molecular rotation rather than vibration. The visco- and piezochromic effects shown in Fig. 4 thus offer solid experimental support to our hypothesis that the RIR process is mainly responsible for the AIE effect.

Thermochromism

Since cooling can also fortify the RIR process, we studied the temperature effect on silole emission.[20] THF is used in the study because of its strong solvating power and low melting point (−108 °C), which can help keep the solute molecules in the solution state at low temperatures. When a THF solution of HPS is cooled, its emission intensity is increased (Fig. 5A). The spectral profile and peak position are virtually unaffected by lowering the temperature, indicating that the emission is still associated with the radiative decay of the singlet excitons but not the triplet ones.

THF has a low viscosity (0.456 cP at 25 °C) with a small temperature coefficient ($\sim$0.008 cP K^{-1}). The enhancement in the PL intensity above the melting point of the solvent thus should not be due to viscosity but a temperature effect. Cooling suppresses the thermally susceptible intramolecular rotations, thus intensifying the HPS emission. Cooling the THF solution to −196 °C using liquid nitrogen brings about a big jump in the PL intensity. The liquid solution must have been frozen into a solid "glass" at such a cryogenic temperature.

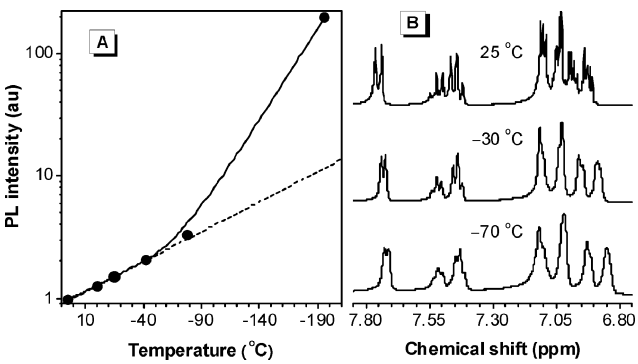

Fig. 5 (A) Effect of temperature on PL intensity of HPS in THF. (B) ^{1}H NMR spectra of HPS in dichloromethane-d_2 at different temperatures. Reproduced with permission from ref. 20. Copyright (2003) American Chemical Society.

In the solid matrix, molecular rotations are greatly restrained and the PL is hence dramatically enhanced.

To experimentally verify the RIR process, dynamic NMR spectra are taken. The fast conformational exchange caused by the rapid intramolecular rotation at room temperature leads to sharp NMR peaks, which can be broadened by cooling, as the rotation slows down at lower temperatures. As anticipated, the HPS solution exhibits sharp NMR resonance peaks at ambient temperature, which are broadened by decreasing temperature (Fig. 5B).[20] The dynamic NMR spectral data confirm that the intramolecular rotation has indeed been restricted at the low temperatures.

Fluorescence decay dynamics

Lifetime is an important kinetic parameter for PL decay. The emission behaviour of HPS can be investigated using a time-resolved technique. The enhancement in HPS emission in water–dimethylformamide (DMF) mixture is accompanied by a corresponding change in the lifetime (Table 1).[25] In pure DMF, the excited state relaxes in a single-exponential manner, with all the excited molecules decaying *via* the same pathway. The PL lifetime is 40 ps, close to the resolution limit of the apparatus (~25 ps), indicative of fast non-radiative annihilation of the excited state.

With the addition of water into DMF, the excited state starts to decay *via* two relaxation pathways. In the mixture with 30% water, 80% (A_1) and 20% (A_2) of the excited HPS molecules decay *via* the fast and slow channels with lifetimes of 0.10 ns (τ_1) and 3.75 ns (τ_2), respectively (Table 1, no. 2).[25] With an increase in the water content in the solvent mixture, the decay *via* the fast channel is slowed down, and the excited molecules decaying *via* the slow channel are populated. In the mixture with 90% water, the excited states decay mainly *via* the slow channel and the lifetime for the slow component is as long as 7.16 ns (Table 1, no. 4).

The PL lifetime of HPS also becomes longer upon cooling, especially when its solution is cooled to below the melting point of DMF (~198 K) where the intramolecular motion is effectively suppressed (Table 1, nos. 5–8).[25] At 150 K, the PL lifetime for the fast decay fraction is 1.23 ns, while that of the slow component is 7.19 ns. At 30 K, the lifetime is lengthened to 10.39 ns, which is about 260-fold longer than that at room temperature. Similarly, the PL lifetime of HPS changes with a variation in the solvent viscosity. The PL decay time is longer in the solution with a higher viscosity.[25]

Table 1 Fluorescence decay parameters of HPS solutions[a]

No.	Solvent[b]	T/K	A_1 (%)	A_2 (%)	τ_1/ns	τ_2/ns
1	H_2O–DMF (0 : 10)	295	100	0	0.04	—
2	H_2O–DMF (3 : 7)	295	80	20	0.10	3.75
3	H_2O–DMF (7 : 3)	295	50	50	0.82	4.98
4	H_2O–DMF (9 : 1)	295	43	57	1.27	7.16
5	DMF	295	100	0	0.04	—
6	DMF	200	51	49	0.31	2.89
7	DMF	150	43	57	1.23	7.19
8	DMF	30	34	66	2.49	10.39

[a] Determined from $I = A_1\exp(-t/\tau_1) + A_2\exp(-t/\tau_2)$, where A and τ are the fractional amount and fluorescence lifetime of the shorter (1)- and longer (2)-lived species, respectively. [b] Volume ratios given in parentheses for solvent mixtures. Adapted with permission from ref. 25*b*. Copyright (2005) American Chemical Society.

In the less viscous solvent at room temperature, the silole molecules are dissolved as isolated species. Little restriction is imposed on their intramolecular rotation. The A_1 value is thus unity, indicating that the HPS molecules are all in the same environment and decay through the same pathway. The decay is awfully fast due to the efficient annihilation process associated with the active intramolecular rotation. Increasing viscosity and decreasing temperature fortify the RIR process and activate the radiative decay. These results all support the RIR model for the AIE effect.

The theoretical work carried out by Shuai's group further verifies our RIR hypothesis.[26] Employing the first-principle calculation to simulate the excited states, the researchers have found that the low-frequency twisting motions of the phenyl peripheral rings of siloles lead to non-radiative decay, which can be alleviated by solution thickening, aggregate formation, and solid-state packing.

Structural tuning

All the *external* control experiments described above prove that the AIE effect stems from the RIR process and that the silole emission can be modulated by physical and engineering manipulations. We proceeded further and tried to exercise an *internal* control on the silole emission. It was rationalized that if our proposed RIR model is correct, impeding intramolecular rotation by chemical means or structural design at the molecular level should make the silole luminogens emissive even in the solution state.

To molecularly activate the RIR process, we attached two isopropyl groups to the peripheral phenyl rings of HPS (**9**).[27] The isopropyl groups are bulky and can effectively obstruct the intramolecular rotation of the phenyl rings. As expected, **9** behaves differently from its HPS parent and emits efficiently in the solution state (Fig. 6). In a dilute acetone solution, **9** emits a strong green light with a Φ_F value of 83%. This PL efficiency is 2–3 orders of magnitude higher than those of the "normal" siloles, which fall in the range of 0.031–0.51%, with a typical value of ~0.1%.[20,21,27]

The introduction of the bulky isopropyl groups significantly alters the dynamics of the singlet excited states of the silole derivatives. Whereas the excited state of HPS rapidly decays with a PL lifetime as short as 40 ps (*cf.*, Table 1), the excited species of **9** relaxes much more slowly with a PL lifetime as long as 6.18 ns.[27] The change in the PL dynamics is in nice agreement with that in the PL efficiency.

The barrier against rotation experienced by the isopropyl-substituted phenyl rings in **9** is estimated to be ~100 kcal mol^{-1}. This high barrier makes it practically impossible for **9** to undergo intramolecular rotation.[27] It is known that a conformationally stiffer chromophore is often a brighter emitter. The structural rigidification caused by the high rotation barrier has clearly played a decisive role in making **9** emissive in solution. This internal control experiment evidently demonstrates that the PL behaviour of silole molecules can be readily tuned by structural tailoring or molecular engineering.

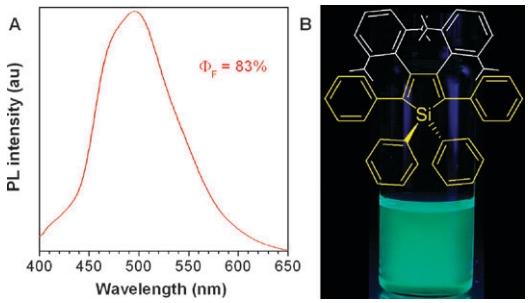

Fig. 6 (A) PL spectrum of a sterically hindered HPS derivative (**9**) in acetone and (B) chemical structure of **9** and photograph of its solution taken under illumination with a UV lamp. Reprinted with permission from ref. 27. Copyright (2005) American Chemical Society.

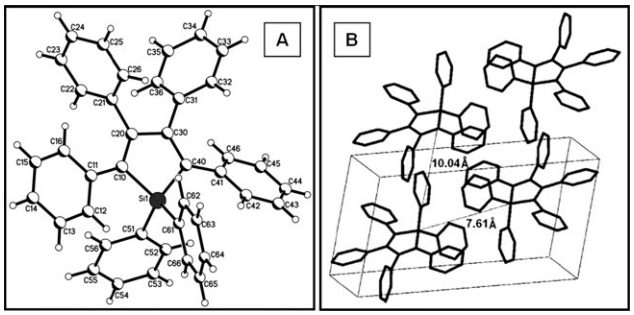

Fig. 7 (A) ORTEP drawing of HPS. (B) Packing diagrams of HPS crystals, where the inter-plane distance is 10.04 Å and the intermolecular distance within the unit cell is 7.61 Å. Reproduced with permission from ref. 28. Copyright (2005) Springer.

Morphochromism

One issue is still outstanding: why does the PL spectrum of HPS red shift when the water fraction in the acetonitrile–water mixture is increased from 80% to 90% (*cf.*, Fig. 2A)? Careful inspection of the absorption spectra of HPS shown in Fig. 3A reveals that the light-scattering effect in the long wavelength region is stronger in the solvent mixture with 80% water than that in the mixture with 90% water. The particle size analysis indicates that the aggregates in the former mixture are bigger in size (196 nm) than those in the latter (130 nm; *cf.*, panels B and C of Fig. 3).

We speculate that the aggregates in these solvent mixtures have different morphological structures. In the mixture with "low" water content, HPS molecules may steadily assemble into crystalline clusters, whereas in the mixture with "high" water content, the molecules may abruptly agglomerate into amorphous aggregates. Transmission electron microscope (TEM) and electron diffraction (ED) measurements confirm that this is indeed the case: the silole aggregates formed in the mixtures with "low" and "high" water contents are crystalline and amorphous, respectively.[28]

Crystallization usually bathochromically shifts PL spectra, but why is the opposite effect observed in the silole system? Analyses of conformation structure and packing arrangement of the HPS molecules in the crystalline phase offer some clues. In the crystals, the silole molecules take a highly twisted fan-like conformation (Fig. 7A).[20] The peripheral phenyl rings are twisted out of the silacyclopentadiene plane to varying extents, with typical dihedral angels of $\sim 30^\circ$ for the phenyl plates at the ring positions next to the silicon atom (C2 and C5 positions) and larger twists of $\sim 70^\circ$ at the C3 and C4 positions. The sp^3 hybridization of the silicon atom makes the phenyl rings attached to it completely out of the plane of the core. The nonplanarity caused by the steric repulsion between the neighboring phenyl plates at the ring carbon atoms and the sp^3 hybridization of the silicon atom at the ring bridge reduces the intermolecular interactions and thus the likelihood of excimer formation. The physical confinement in the crystal lattice greatly rigidifies the molecular conformation of HPS, thereby increasing its PL efficiency in the solid state.

The unusual blue shift observed in the crystalline phase is attributable to the conformation twisting in the crystal packing process, during which the silole molecules conformationally adjust themselves in order to fit into the crystalline lattice. Without this restraint, the silole molecules in the amorphous phase may assume a more planar conformation and thus show a redder luminescence. The conformational difference in the amorphous and crystalline phases is evidently the origin of the unusual morphochromism. The large inter-plane (~ 10 Å) and intermolecular (~ 7.6 Å) distances in the crystal unit cell (Fig. 7B) manifest the lack of strong chromophore interactions that tend to induce non-radiative relaxations and red shifts as seen in the conventional crystals with π–π stacking interactions.

New AIE systems

The mechanistic studies above make the AIE picture clear. In solution, the multiple aryl blades of the silole molecules rotate around the single-bond axles linking the peripheral aryl rotors and the central stator of the silacyclopentadiene core. The intramolecular rotation converts photonic energy to heat and deactivates the excited states non-radiatively, thus making the molecules non-emissive. In the aggregates, the intramolecular rotation is restricted and the non-radiative relaxation channel is obstructed. Thanks to their propeller-like shapes, the silole molecules experience little π–π stacking interaction in the condensed phase and thus have little chance to form excimer species. The activated RIR process and the reduced likelihood of excimer formation cooperatively make the silole molecules highly emissive in the solid state.

This mechanistic picture predicts that the AIE effect should not be a special attribute of the silole molecules but a common property of many luminogens with similar structural features. Guided by the mechanistic understanding, we synthesized a large number of luminogens with propeller-shaped molecular structures. We systematically studied their PL behaviour with the aim of developing new AIE systems and gaining more insight into AIE processes.

Some examples of the luminogens we have prepared and studied are given in Chart 3. All the molecules show typical AIE behaviour, that is, they are non-emissive in solution but highly luminescent as aggregates.[29] Like the silole derivatives, these molecules are propeller-shaped, consisting of multiple phenyl rotors and olefinic or aromatic stators. Their AIE

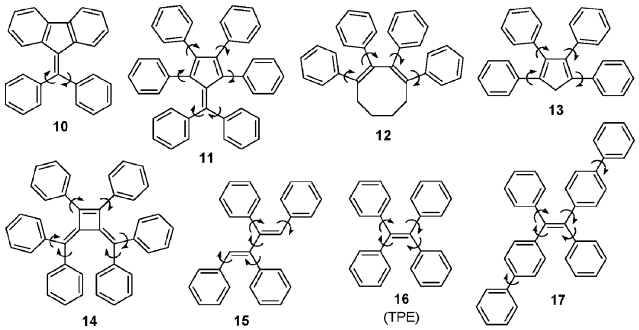

Chart 3 Examples of pure hydrocarbon AIE fluorophores developed in our laboratories.

behaviour thus must stem from RIR processes in their aggregates.[20,21] Molecules **10–17** comprise only carbon and hydrogen atoms and contain neither heteroatoms nor polar units. This structure feature unambiguously excludes the involvement of J- and H-aggregates and the TICT effect in their PL processes.

If an RIR process is a decisive factor in determining whether a luminogen is AIE active, polyphenylenes with phenyl rings directly strung together by single bonds without olefinic linkers should also exhibit AIE properties. This is indeed the case: the polyphenylenes shown in Chart 4 (**18–20**) are all AIE luminogens.[29] In comparison to the cyclic olefins given in Chart 3, the polyphenylenes are easier to synthesize. As a matter of fact, many polyarylenes are even commercially available. The demonstration of AIE activity for **18–20** thus opens a wide avenue to many readily accessible AIE systems.

We further proceeded to explore heteroatom AIE systems containing polar functional groups. Although the AIE effect is not activated by the processes associated with the interactions between the functional groups, such as push–pull polarization, introduction of the polar groups into the molecular structures of AIE luminogens greatly enriches the palette and makes the emissions more "colourful".[30] Through covalent decoration of the AIE cores with various functional groups, a series of new luminogens with emission colours covering the entire visible spectral region (from blue to green to yellow to orange to red) have been developed (Chart 5).

Some of the luminogens can emit light of multiple colours. For example, aggregates of butterfly-shaped pyran derivative **28** formed in THF–water mixtures with 40%, 90% and 99% water emit green, orange and red light, respectively (Fig. 8). Thanks to the chiral cholesteryl wings attached to the pyran skeleton, the molecules of **28** self-assemble to form crystalline, helical aggregates under appropriate conditions, which emit polarized light with high efficiency.[30*a*] This demonstrates the ready tunability of the PL colour by simple means, that is, changing the composition of the aqueous mixture.

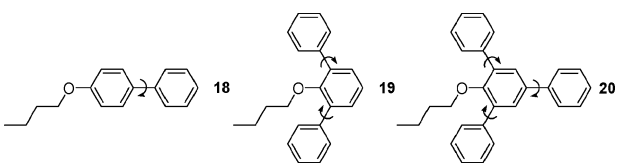

Chart 4 Examples of polyphenylene AIE fluorophores developed in our laboratories.

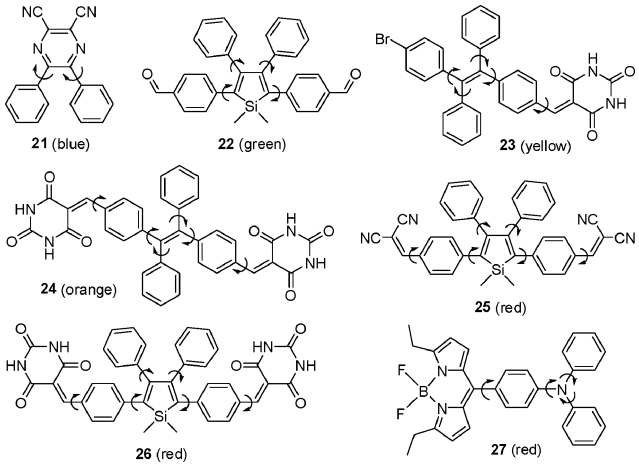

Chart 5 Examples of heteroatom-containing AIE fluorophores that emit visible light of various colours.

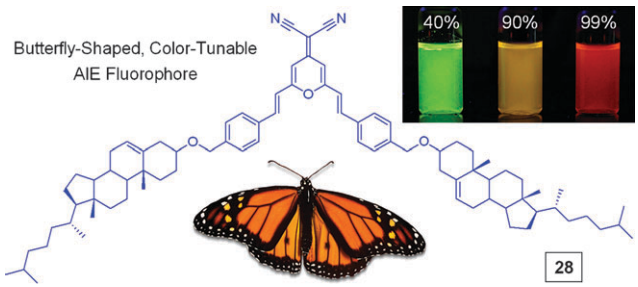

Fig. 8 The nanoaggregates of butterfly-shaped AIE fluorophore **28** suspended in THF–water mixtures with water contents of 40%, 90% and 99% emit green, yellow and red light, respectively, under UV light illumination. Adapted with permission from ref. 30*a*. Copyright (2007) American Chemical Society.

Further mechanistic evidence and insight

All the examples of luminogens shown in Charts 3–5 were designed according to our mechanistic understanding of the silole system. The feedback that all of these luminogens are AIE active not only widens the territory of AIE study but also substantiates our RIR hypothesis. The new AIE systems offer new materials for further studies, which may help to discover new photophysical phenomena and collect more mechanistic information.

While we had encountered synthetic difficulties in our early attempt to lock the peripheral phenyl rings in HPS by covalent bonds, it is easy to link together the neighbouring phenyl rings in **10** by a single bond. The diphenyldibenzofulvene derivative with two rotatable phenyl rings displays typical AIE features. In sharp contrast, its ring-closed form (**29**) behaves oppositely: its emission is quenched by aggregate formation.[30*b*]

A dilute solution of **10** in acetonitrile gives very weak PL but in an aqueous mixture with 99% water, it emits strongly in a 35-fold higher efficiency (Fig. 9A). On the other hand, the ring-closed form **29** emits an intense blue light at 447 nm in its acetonitrile solution (Fig. 9B). Its Φ_F value is decreased by $\sim$7 times upon addition of 99% of water into its solution. Evidently, fixing one of the phenyl rotors in **10** by a single bond on the dibenzofulvene stator switches off its AIE features and turns it into a "conventional" fluorophore (**29**).[30*b*]

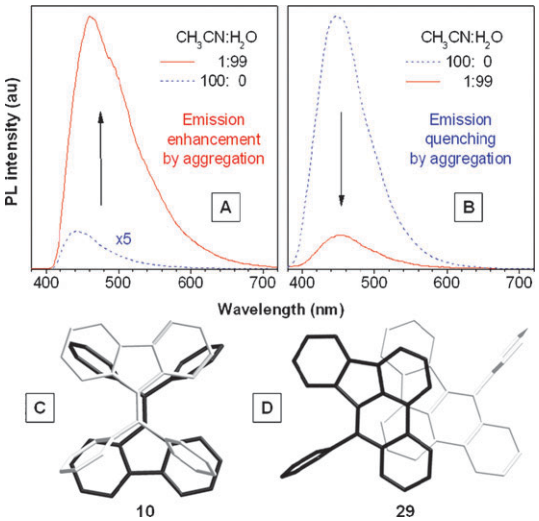

Fig. 9 PL spectra of (A) **10** and (B) **29** in acetonitrile and its aqueous mixture (99 vol% water). Top view of the dimer structures of (C) **10** and (D) **29** extracted from their X-ray crystal analysis data. Reproduced with permission from ref. 30. Copyright (2007) American Chemical Society.

The emission spectrum of the crystals of **10** is blue-shifted as compared to that of its solution, similar to what is observed in the HPS system. On the other hand, the emission spectrum of the crystals of **29** contains a shoulder peak in the red spectral region at 509 nm. In the dimer structure extracted from the crystal analysis data, the dibenzofulvene stator and the phenyl rotors of the molecules of **10** are arranged in an antiparallel fashion, with little involvement of π–π stacking interactions (Fig. 9C).[30b] The big, flat benzo[*e*]acephenanthrylene stator of **29**, however, allows direct stacking of two adjacent molecules. The face-to-face stacking leads to strong π–π interactions between the stators and promotes excimer formation, thus weakening and red-shifting the emission of **29** in the crystalline phase.[30b]

As stated above, when a non-emissive molecule is induced to emit by aggregate formation, the molecule is referred to as "AIE active". During our exploration of new luminogens, we have found that the emissions of some luminescent molecules are enhanced by aggregation. In other words, they exhibit an aggregation-induced emission enhancement (AIEE) effect. For example, **30** and **31** are luminescent in solution, but their aggregates are more emissive (Fig. 10).[29]

The emissions of **30** and **31** are due to the fluorescence of their carbazole chromophores. Intuitively, one would expect **30** to be more emissive than **31** because the former contains more carbazole units than the latter. In reality, however, **30** is less emissive ($\Phi_F \sim 16\%$) than **31** ($\Phi_F \sim 30\%$) in THF at room temperature.[29] The carbazole ring is not only a chromophore but also a rotor in **30** and **31**. The emission of **30** thus must be weakened to a larger extent by the more active intramolecular rotation of its multiple carbazole rotors in solution.

When the solutions are cooled to −70 °C, **30** shows a stronger AIEE effect than **31**: the emission of the former is enhanced to a higher degree than that of the latter (Fig. 10).[29] As discussed above, cooling suppresses molecular motion and

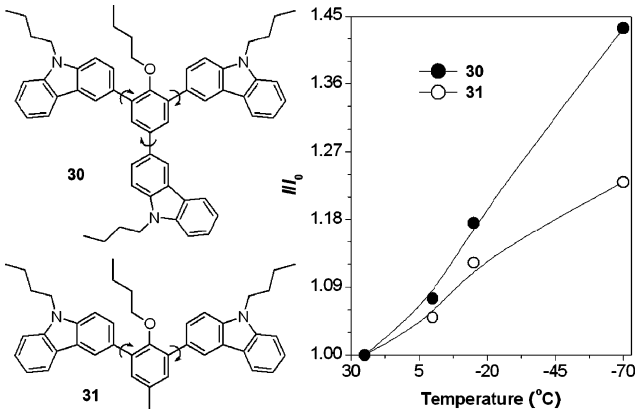

Fig. 10 Effects of temperature on PL intensities of dilute solutions of **30** and **31** in THF. Reproduced with permission from ref. 29. Copyright (2007) The Royal Society of Chemistry.

activates the RIR process. Because **30** contains more rotors, its emission is thus more sensitively affected by the temperature effect. This further manifests that the RIR process plays a crucial role in boosting PL efficiency.

The activation of the RIR process implies the molecular conformation has rigidified. The structural stiffening caused by the fixation of the aromatic plates due to the environmental constraints in the aggregates may lead to polarized emission. Indeed, emission anisotropy is observed in AIE systems. As can be seen from Fig. 11A, the emission of the amorphous aggregates of silole **32** is stronger in the vertical direction (I_v) than in the horizontal direction (I_h). Its emission anisotropy is greatly enhanced in the fibrous aggregates, probably due to the more rigid molecular conformation and better luminogenic alignment in the microfibers.

The conformational stiffening and luminogenic orientation should be further enhanced in the crystalline aggregates as the molecules are confined in the crystalline lattice. The emission anisotropy thereby should be larger in AIE crystals. While the molecules of **32** do not crystallize, those of its congener with more phenyl rings (**8**) form large crystals. As expected, I_v is much higher than I_h in the crystals of **8** ($I_v/I_h \sim 4.5$). The PL anisotropy of the crystalline aggregates is ~3.9-fold higher than that of the amorphous ones (compare panels C and D of Fig. 11), demonstrating a remarkable morphology effect on the PL behaviour of AIE aggregates.

Crystallization-induced emission

In many of the AIE systems we have studied, crystallization leads to enhanced emission.[27,31] This effect of crystallization-induced emission enhancement is again opposite to the effect observed in conventional luminophores, where crystallization commonly weakens or quenches emission.[2–5] Further studies in the area lead to the development of even more intriguing systems, that is, ones that display crystallization-induced emission (CIE), where non-emissive molecules are induced to emit by crystallization but not amorphization. An example of a CIE system is shown in Fig. 12.[32] In dilute acetonitrile solution, **33** is virtually non-luminescent. Its molecules crystallize in the acetonitrile–water mixture with ~60–70% water, and the crystallization turns **33** into a strong emitter. However, its

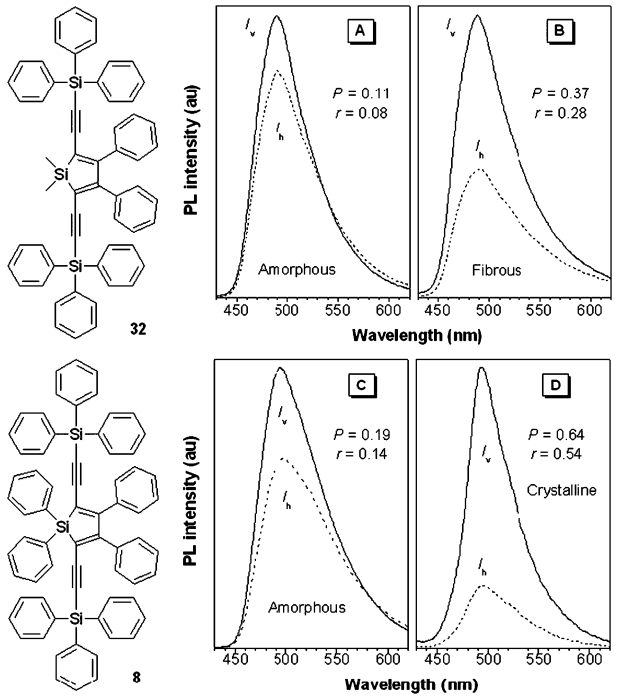

Fig. 11 Polarization in the emissions of (A) amorphous and (B) fibrous aggregates of **32** and (C) amorphous and (D) crystalline aggregates of **8**. Degree of polarization (P) and emission anisotropy (r) are determined by $P = (I_v - I_h)/(I_v + I_h)$ and $r = (I_v - I_h)/(I_v + 2I_h)$, where I_v and I_h are the PL intensities in vertical and horizontal directions, respectively.

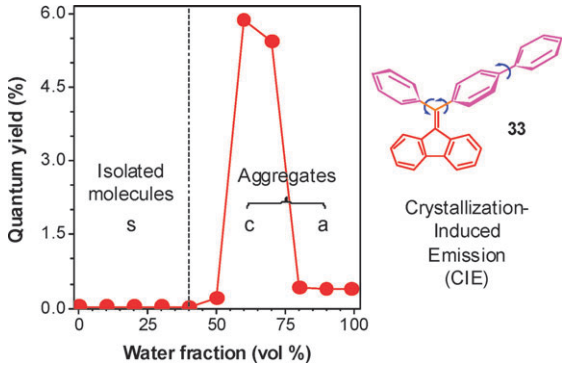

Fig. 12 Crystallization-induced emission: plot of quantum yield of **33** against the solvent composition of an acetonitrile–water mixture. Abbreviations: s = solution, c = crystalline aggregate, and a = amorphous aggregate. Reproduced with permission from ref. 32. Copyright (2007) The Royal Society of Chemistry.

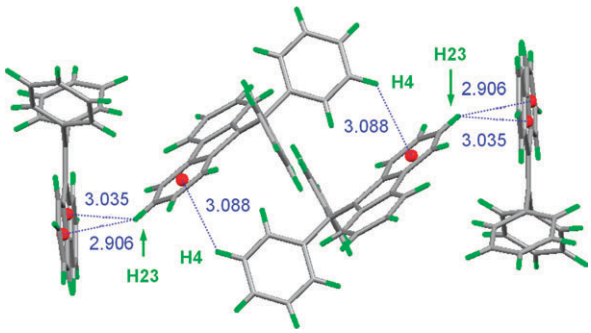

Fig. 13 Perspective view of the packing arrangements in crystals of **10**. Aromatic C–H···π hydrogen bonds are denoted by dotted lines. Adapted with permission from ref. 30*b*. Copyright (2007) American Chemical Society.

nanoaggregates formed in aqueous mixtures with very high water content ($\geq 80\%$) are amorphous and are only weakly luminescent.

Molecules of **33** are geometrically asymmetric. Because of this structural feature, there exist many molecular voids and large free volumes in the amorphous aggregates of **33** that may allow its phenyl rings to rotate even in the solid state, taking into account that the rotational motion requires little energy, as even microwave irradiation can cause molecules to rotate. However, in the crystalline phase, the molecules of **33** enter into, and are fastened by, the crystalline lattice. This strengthens the RIR process, thereby making the crystals of **33** emissive.[32]

Noncovalent molecular interactions are frequently involved in the crystallization process to assist the molecules to orient and assemble. As can be seen from the example of a crystal packing arrangement shown in Fig. 13, there exist many C_{Ar}–H···π bonds between the phenyl rotors and the dibenzofulvene stators in the crystals of **10**. Multiple "hydrogen bonds" of this kind collectively can greatly stiffen molecular conformation and luminogen arrangements. As a result, the crystals become highly fluorescent.[30*b*]

Phosphorescence from a pure organic molecule has seldom been observed under ambient conditions, partially due to PL quenching by molecular motion during the long lifetime of the triplet state.[33] Organic phosphorescence has commonly been measured at cryogenic temperatures (*e.g.*, 77 K) in frozen "glasses" of organic solvents or solvent mixtures (*e.g.*, an ether, isopentane and ethanol or EPA mixture), in which molecular motion is suppressed.[2,3] Since crystallization can also impede molecular motion, it may enable the organic phosphorescence to occur at room temperature.

Crystallization-induced phosphorescence (CIP) is observed in benzophenone (**34**). This molecule is non-emissive at room temperature. Its crystals, however, emit a blue light of 448.5 nm with an average lifetime of 316.5 μs in an efficiency of ~16% (Fig. 14A). The crystals of its fluorinated derivative (**35**) also emit a blue light with a long lifetime with high efficiency under ambient conditions. Similar results are obtained from the crystals of other molecules such as 4,4′-dibromobiphenyl (**36**) and diphenylacetylene (**37**), indicative of the generality of the CIP phenomenon.

All the molecules are known to be phosphorescent at low temperatures.[33] The emission spectra of their crystals taken under ambient conditions match those measured at low temperatures well. For example, the PL spectrum of the crystals of **34** resembles the phosphorescence spectrum of its solution at 77 K, while the PL spectrum of its ethanol solution is hardly discernable at room temperature (Fig. 15A). The PL of **35** decays double-exponentially, with an average lifetime of 1.3 ms (Fig. 15B). This very long lifetime further proves that the emission is phosphorescence but not fluorescence.

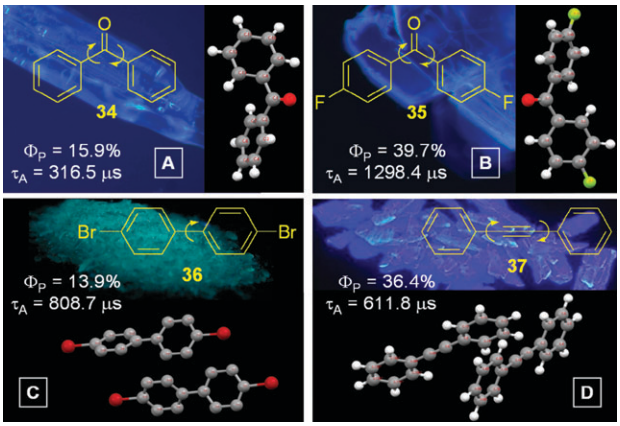

Fig. 14 Examples of phosphors with crystallization-induced emission (CIE) attributes: chemical structures, phosphorescence quantum yields (Φ_P), average lifetimes (τ_A), molecular structures, and crystalline packing arrangements of (A) benzophenone (**34**), (B) 4,4′-difluorobenzophenone (**35**), (C) 4,4′-dibromobiphenyl (**36**) and (D) diphenylacetylene (**37**). Photographs of the phosphorescent crystals were taken under illumination of a handheld UV lamp.

The microcrystals formed by crushing the big crystal plates of **35** are still luminescent, even after exposure to oxygen and immersion in water. On the other hand, its solid deposit on a TLC plate or a filter paper is non-emissive at room temperature. It becomes luminescent when cooled to 77 K but returns back to the non-emissive state when warmed to room temperature. The results of these control experiments suggest that the light emission is quenched not by the molecular collisions and the interactions with oxygen and water but by intramolecular motion, noting that all these molecules comprise of rotatable phenyl blades.

AIE and TICT

Like AIE, TICT is associated with intramolecular rotation or twisting. However, unlike AIE, TICT results in PL diminution. TICT generally occurs in a luminogen system containing D and A units with push–pull interactions. In a polar solvent, the charge-separated conformation resulting from intramolecular twisting is stabilized by the solvation effect, whose excited state often decays non-radiatively.[34] This is a drawback if one wishes to use the luminogen as a fluorescent biosensor, because biological processes basically occur in aqueous medium. The emission colour of an AIE luminogen is scarcely affected by solvent polarity, whereas that of a TICT luminogen typically bathochromically shifts with increasing solvent polarity, as polar solvents alter its ground and excited states and narrow its energy gap.[34,35]

In the mechanistic discussions above, we have excluded the involvement of TICT in the silole-based AIE systems.[20,21] However, when polar heteroatoms, especially D/A groups, are introduced into an AIE system, the TICT process comes into play. For example, **27** contains a D–A pair of triphenylamine–boradiazaindacene (BODIPY) with multiple aryl rotors.[36] This structural feature is likely to make **27** both AIE and TICT active. As shown in the upper panel of Fig. 16, the PL colour of **27** is very sensitive to the solvent polarity. As the solvent is changed (hexane → toluene → chloroform → methanol), its PL colour is changed accordingly (green → yellow → red → infrared). A similar trend in the colour change is observed in the emission of another BODIPY derivative **38**, which is a cousin of **27** with the phenyl bridge replaced by a biphenyl one. The remarkable solvent effects on the emission colours of **27** and **38** confirm the involvement of TICT in their PL processes.

Blending water with THF in different ratios gives aqueous mixtures with varying solvent polarity and solvating power. While **38** gives a PL spectrum which peaks at ~685 nm in pure THF, the spectrum is dramatically weakened in intensity and the PL peak is red-shifted to ~700 nm in the THF–water mixture with 10% water, due to an increase in solvent polarity (Fig. 17A). The emission remains weak when the water content in the THF–water mixture is increased to 65%, after which the PL intensity starts to increase, accompanied by a blue-shift in the PL peak (Fig. 17). In the solvent mixture with 99% water, the PL intensity is ~70-fold higher than that in the mixture with 50% water, with the PL peak blue-shifted to ~658 nm.

When the water content is increased, the aqueous mixture becomes more polar. The emission from the TICT luminogen should be monotonically decreased and red-shifted, but why are the opposite effects observed in the high water-content region? Accompanying the increase in the water content, the solvating power of the mixture is decreased. At a certain point with an appreciably high water content, the solvating power of the aqueous mixture has deteriorated to such an extent that it cannot dissolve all the luminogen molecules any more. Some

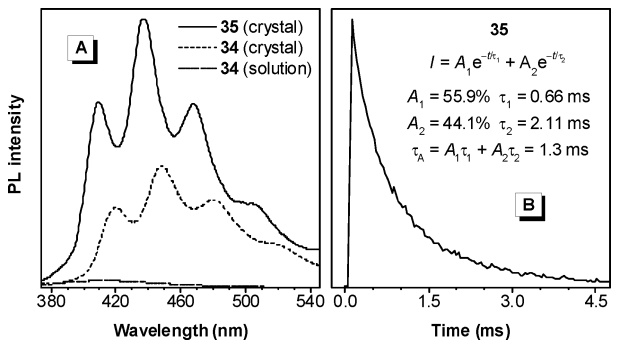

Fig. 15 (A) PL spectra of **34** and **35** in the crystalline and solution states at room temperature. (B) PL decay curve of crystals of **35** and associated dynamic parameters.

Fig. 16 Photographs of boradiazaindacene (BODIPY) derivatives **27** (upper panel) and **38** (lower panel) taken under illumination of a UV lamp in solvents with increasing polarity (from left to right): (A) hexane, (B) cyclohexane, (C) toluene, (D) chloroform, (E) ethyl acetate, (F) THF, (G) ethanol, (H) acetonitrile, and (I) methanol.

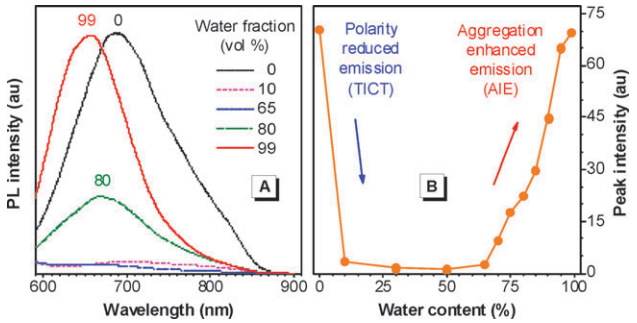

Fig. 17 (A) PL spectra of BODIPY derivative **38** in the THF–water mixtures with different water contents. (B) PL peak intensity of **38** *versus* water content of the solvent mixture.

of the molecules thus begin to aggregate into nanoparticles, whose polarity inside is lower than that outside.

Accompanying aggregate formation, the environmental polarity of the luminogens is decreased and in the meantime the RIR process is activated. The decreased polarity blue-shifts the PL peak of **38** (*cf.*, Fig. 16), while the RIR process boosts its PL intensity. In the aqueous mixture with very high water content (*e.g.*, 99%), the AIE effect predominates. It overcomes the detrimental TICT effect and turns **38** into a strong red emitter. The BODIPY-based luminogens are promising for biosensor applications because of their long wavelength emissions and high PL efficiencies. The demonstration that the BODIPY luminogens with the "right" molecular structures[36] are AIE active points to a new direction in the search for efficient turn-on biosensor systems.[37]

Applications

Light emitters are useful materials and have found a variety of technological applications. Great current interest is focused on the exploration of their utilities in the development of OLEDs and sensory systems. Many research groups have worked on the impediment of luminophore aggregation in an effort to fabricate efficient OLEDs, while other groups are developing luminescence turn-off sensors by utilizing the ACQ effect, in which the luminophores are incorporated into biological and chemical systems as labels *via* chemical attachment or probes *via* physical mixing.[8] The labels/probes are initially dissolved and hence emissive (on) but become non-emissive (off) when they are induced to aggregate by the changes in the analytes.[38]

The AIE luminogens are highly emissive in the aggregated state. This unique characteristic differentiates them from conventional luminophores and makes them ideal candidates for high-tech applications in the practically useful solid state.[20–32] While many possibilities can be imagined for AIE systems, we have mainly explored their applications as luminescence sensors and in light-emitting devices.

Chemical sensors

We first checked the possibility of using AIE luminogens as chemosensors for the detection of volatile organic compounds (VOCs), which has hygienic and environmental implications. As shown in Fig. 18, the light emission from a spot of **17**, a diphenylated tetraphenylethene (TPE) derivative, on a TLC plate (panel B) is turned off when the plate is put into a Petri-dish set saturated with chloroform vapour (panel C).[31c] The spot becomes emissive again when the solvent is evaporated. A similar effect is observed in other VOCs (dichloromethane, acetonitrile, acetone, THF, *etc.*) and with other AIE luminogens (HPS, MPPS, TPE, *etc.*).

The solvent vapor may have condensed and formed a thin liquid layer on the surface of the TLC plate, which dissolves the adsorbed luminogen molecules and consequently quenches their light emission. After solvent evaporation, the molecules aggregate and hence emit again. This luminescence "off/on" switching is completely reversible and reliably repeatable many times, because the involved process is a non-destructive physical cycle of dissolution (deaggregation)–aggregation.

To learn more about the VOC-sensing process, changes in the PL spectra of HPS and MPPS films in atmospheres of VOC vapours are followed by spectroscopic methods. A thin film of the silole was coated on the inner wall of a quartz cell and several drops of acetone liquid were added in a small container placed on the bottom of the cell. Similar to the observation on the TLC plate, the emission of MPPS becomes weaker and is almost completely quenched after exposure to the acetone vapour for ~2 min (Fig. 19A). However, the PL of the HPS film becomes stronger and is blue-shifted after fuming with the solvent vapour (Fig. 19B). This demonstrates that the vapochromism can be readily tuned by changing the molecular structure of the AIE luminogen.[28,31a]

But why do HPS and MPPS respond to the solvent vapour in opposite ways? It is well known that solvent vapour can activate the dynamic crystallization process of dye molecules.[39] The morphologies of the siloles before and after the vapour fumigation were thus examined. Scanning electron microscope (SEM) images reveal that the untreated films of both HPS and MPPS are amorphous. After solvent fuming, the MPPS film becomes smoother, while regularly shaped microcrystals are formed in the HPS film. In the ED patterns, the fumed MPPS film displays only a diffuse halo but the fumed HPS film gives diffraction spots, confirming that the former remains amorphous but the latter becomes crystalline.

These results indicate that the acetone vapour has dissolved the molecules in the MPPS film and hence attenuated their light emission. In contrast, the solvent vapour has aided the HPS molecules to crystallize in the supersaturated solution and thus blue-shifted their PL spectrum and intensified their PL intensity. HPS has a symmetric structure and its molecules may pack well during the fuming process. MPPS molecules, on the other hand, are asymmetric in shape and hence are difficult

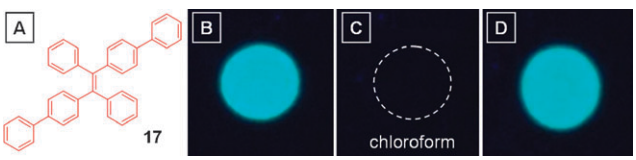

Fig. 18 Spots of (A) 1,2-diphenyl-1,2-bis(4-phenylphenyl)ethene (**17**) on TLC plates placed in Petri-dish sets (B) without and (C) saturated with chloroform vapour. The photograph in panel D was taken after the organic vapour in panel C had been evacuated. Adapted with permission from ref. 31*c*. Copyright (2007) American Institute of Physics.

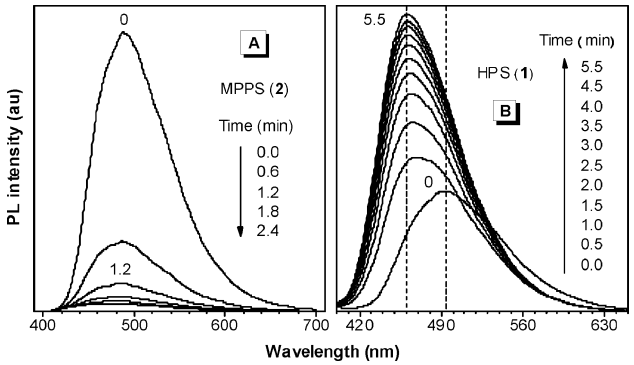

Fig. 19 Effects of acetone vapour on the PL spectra of the films of (A) MPPS and (B) HPS deposited on quartz cells. Adapted with permission from ref. 31*a*. Copyright (2007) Springer.

to pack into crystalline lattices under the solvent vapour. On the TLC plate, however, the HPS molecules are segregated by the fine silica particles and are difficult to crystallize. This explains why the light emission of HPS is quenched on the TLC plate but enhanced on the quartz cell after vapour fumigation.[28,31*a*]

The efficient emission of the AIE aggregates inspired us to develop nanostructured chemosensors for explosives detection. Nitroaromatics such as 2,4,6-trinitrotoluene (TNT) and 2,4-dinitrotoluene (DNT) are warfare explosives, detection of which is of value to homeland security. Due to commercial unavailability of TNT and DNT, picric acid (PA) is used as a model explosive in our investigations.[27,40] The nanoaggregates of aminated HPS derivative **39** are prepared by admixing 1% of its THF solution with 99% water. The emission of **39** is progressively weakened with sequential addition of PA into the aqueous suspension of the silole aggregates (Fig. 20A). The Stern–Volmer plot gives a PL quenching constant (K_{sv}) of 1.67×10^5 M^{-1}. Evidently, the nanoaggregates of **39** work as a sensitive explosive probe.

In aqueous media, molecules of **39** aggregate and emit. When a small amount of acid (*e.g.*, sulfuric acid) is added into water, **39** becomes soluble in water because its amino groups are transformed to ammonium salts. The genuine dissolution of **39** at the molecular level in the acidic medium quenches its emission because of its AIE nature. The PL intensity remains unchanged when the pH value is increased from 2 to 5.4 by the addition of a base but starts to swiftly increase afterwards (Fig. 20B). When the pH value exceeds 5.4, the molecules of $\mathbf{39}^{2+}$ are transformed back to the amine form (**39**). The decrease in the hydrophilicity induces the molecules to aggregate in the aqueous medium and thus turns on the light emission.[40]

The working principle involved in the pH sensing process is the dissolution (deaggregation) and aggregation of an AIE luminogen at the appropriate pH value. Following this mechanism, a fluorescent pH sensor with the opposite response can be readily designed. Thus, the emission of a hydroxylated silole, namely, 1-[2-(4-hydroxyphenyl)ethynyl]-pentaphenylsilole is switched on and off in the low and high pH regions, as the luminogenic molecules are aggregated and deaggregated (or dissolved) in the acidic and basic aqueous media, respectively.[41]

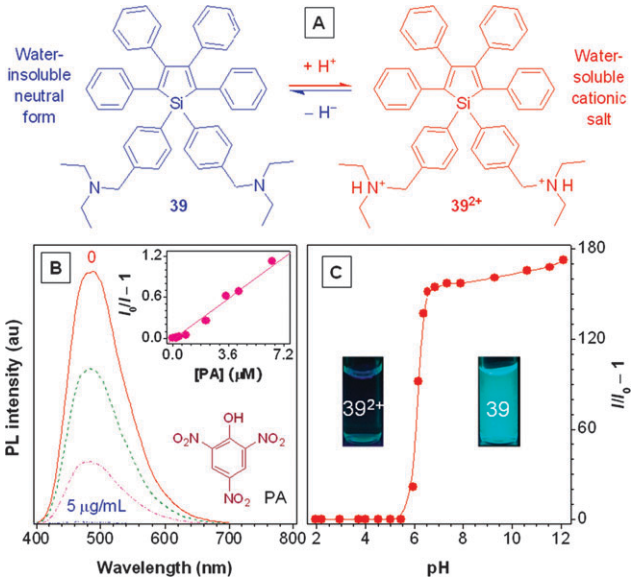

Fig. 20 (A) Aminated HPS derivative **39** and its protonated form $\mathbf{39}^{2+}$. (B) PL spectra of **39** in THF–water mixtures (1 : 99 by vol) containing different amounts of picric acid (PA). Inset: Plot of $I_0/I - 1$ *vs.* [PA]; I_0 = intensity at [PA] = 0 μM. (C) Change in PL intensity of $\mathbf{39}^{2+}$ or **39** with pH value of the aqueous mixture; I_0 = intensity at pH = 2. Inset: photos of the solution of $\mathbf{39}^{2+}$ and the suspension of **39** at pH 2 and 12, respectively, taken under illumination of a UV lamp. Reproduced with permission from ref. 40. Copyright (2007) Elsevier.

Layer-by-layer (LbL) deposition of polyelectrolytes has been widely used to construct functional thin solid films.[42] UV–vis absorption has been used to monitor the assembling process. The method, however, requires that the polyelectrolytes carry chromophores (*e.g.*, polystyrene) and that the substrates are transparent (*e.g.*, quartz). LbL deposition is basically a polymer aggregation process, which thus offers a stage for an AIE luminogen to perform as an *in situ*, real-time monitor.

When a mixture of poly(diallyldimethylammonium chloride) and $\mathbf{39}^{2+}$ is used as a co-cation to assemble with poly(styrenesulfonate) anion by the LbL deposition process on a quartz plate, the emission intensity of $\mathbf{39}^{2+}$ linearly increases with increasing numbers of bilayers (Fig. 21). The same linear calibration curve is obtained when an inexpensive glass plate is used as the substrate.[43] The AIE luminogen is not limited to the examples given in Fig. 21 but can in principle be used as a probe for monitoring assemblies of polyelectrolytes free of chromophores on any substrates, including the technologically useful silicon wafer and mica.

Biological probes

The results obtained in our studies of using AIE luminogens as chemosensors enthused us to further explore their high-tech applications, particularly as bioprobes. Hydrophilic functional groups, such as hydroxyl, amino, ammonium, sulfonate and boronate, are incorporated into the structures of the AIE dyes to make them water soluble. The luminogens are non-emissive in aqueous buffers but become emissive (or turned on) when bound to biological molecules. Such turn-on biosensors are advantageous over their turn-off counterparts. For example, the turn-on sensors are less likely to generate false-positive

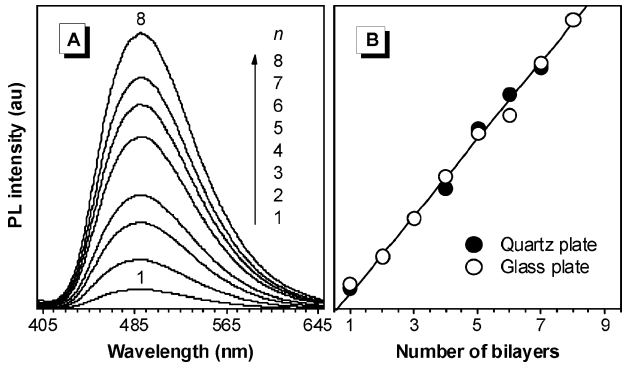

Fig. 21 (A) PL spectra of $[(\mathbf{39}^{2+} + \text{PDDAC})/\text{PSS}]_n$ films with different numbers of bilayers (n) deposited on a quartz plate. Abbreviations: PDDAC = poly(diallyldimethylammonium chloride), PSS = poly(styrenesulfonate). (B) Plots of PL intensities *versus* numbers of bilayers deposited on quartz and glass plates. Adapted with permission from ref. 43*a*. Copyright (2009) Elsevier.

signals.[38] They are more sensitive and faster, as the formation of a few emissive aggregates can be readily discerned by the naked eye from the dark background. This is particularly helpful for on-site trials, field screening and household testing, in which constraints in space, transportation, *etc*. prevent the use of sophisticated instruments.

An example of using AIE luminogens as turn-on sensors for protein assays is given in Fig. 22.[30c] While sulfonated TPE derivative **40** is non-luminescent in a neutral phosphate buffer, its emission is switched on by adding bovine serum albumin (BSA) into the buffer. The PL intensity at [BSA] = 500 mg L^{-1} is ~240-fold higher than that in the absence of BSA. This high sensitivity enables BSA detection at a concentration as low as 0.05 mg L^{-1} or 50 ppb. The plot of the emission intensity as a function of BSA concentration gives a linear calibration curve at BSA concentrations up to 100 mg L^{-1}, indicating that the AIE luminogen can be used for BSA quantitation over a wide concentration range.

Using traditional fluorophores for detection and quantitation of proteins often involves lengthy procedures with carefully timed steps. Some of them show small Stokes shifts and nonlinear curves, while others are even environmentally unstable (*e.g*., fluorescamine). On the other hand, **40** gives a large Stokes shift (>100 nm) and a linear calibration curve over a wide concentration range (up to 100 mg L^{-1}). It is environmentally stable, with no changes in its PL spectra observed after its solution has been stored under ambient conditions without protection from light for more than 2 months. Moreover, conventional fluorophores suffer from a self-quenching problem at high dye concentrations. The PL of **40**, however, is intensified with an increase in concentration, owing to its unique AIE attributes.

How does **40** interact with BSA? We know that the rotational motion of aryl rotors of an AIE luminogen in solution causes its excited state to non-radiatively decay, whereas aggregate formation obstructs the intramolecular rotation. The PL peak of **40** in the presence of BSA is identical to that of its nanoaggregates, indicating that the PL stems from the aggregates. It is unlikely that **40** conjugates with BSA to form a covalent adduct. The interaction between **40** and BSA thus should be mainly hydrophobic in nature.

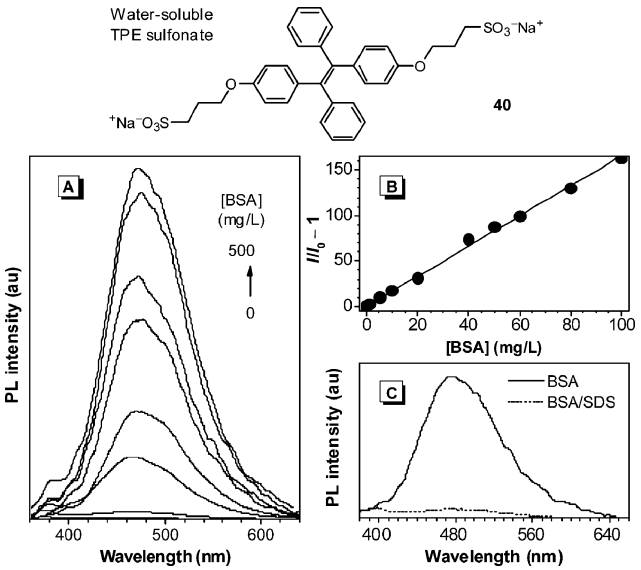

Fig. 22 (A) PL spectra of sulfonated TPE salt **40** in phosphate buffer (pH = 7.0) containing different amounts of bovine serum albumin (BSA). (B) Plot of [BSA] *versus* $I/I_0 - 1$; I_0 = intensity at [BSA] = 0 mg L^{-1}. (C) Effect of BSA on the PL spectrum of a buffered solution of **40** in the absence and presence of sodium dodecyl sulfate (SDS). Reproduced with permission from ref. 30*c*. Copyright (2007) American Chemical Society.

There exist hydrophobic binding sites such as hydrophobic pockets in the native folding structure of BSA chains.[44] The molecules of **40** may bind to the hydrophobic regions of the BSA chains and enter into hydrophobic cavities of their native folding structures, which activate the RIR and AIE processes. Sodium dodecyl sulfate (SDS) is known to unfold protein structure effectively. Addition of SDS into the BSA solution of **40** dramatically weakens its emission (Fig. 22C). The SDS molecules may have destroyed the native folding structure of the BSA chains by binding to the hydrophobic regions of the protein. The molecules of **40** are released back to the buffer solution and cease to function as a protein probe. The AIE bioprobe is thus native-conformation sensitive, which offers the opportunity to visualize hydrophobic pockets of proteins, active sites of enzymes, *etc*. which remain mysterious because of the difficulty in "seeing" their real "faces".

In traditional fluorescence immunoassay (FIA) systems, the fluorophore to protein (F/P) ratios are often low because of the problems caused by the notorious self-quenching effect. When several fluorophoric labels are attached to one antibody, the fluorophores are located in close vicinity, which activates energy transfer and decreases the PL intensity and efficiency. The AIE effect permits the use of high F/P ratios and the AIE luminogens can thus serve as powerful immunosensors. Biofunctionalized HPS nanocrystals are used in our FIA study, which are prepared by the procedures shown in Fig. 23A. The HPS crystals are ball-milled in a mixture of hydroxypropyl cellulose and SDS in water (step 1). After encapsulation with polyelectrolyte multilayers (step 2), specific immunoreagents such as antibodies are attached to the nanocrystals (step 3). The nanocrystal core is comprised of a huge number of HPS molecules, while the encapsulated crystal

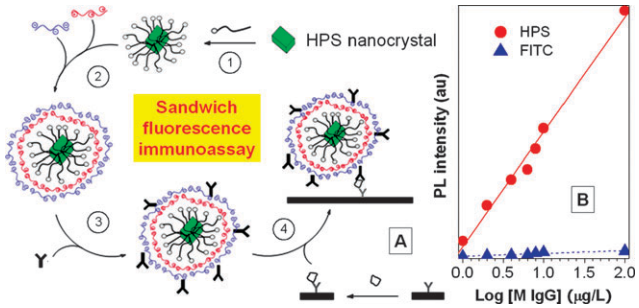

Fig. 23 (A) Schematic illustration of a sandwich-type immunoassay process using polyelectrolyte-encapsulated, antibody-functionalized HPS nanocrystals as a fluorescent bioprobe. (B) Plot of PL intensity of HPS nanocrystals functionalized with goat anti-mouse immunoglobulin G *versus* the concentration of mouse immunoglobulin G (M IgG). Data for the system using fluorescein isothiocyanate (FITC) as bioprobe are shown for comparison. Reproduced with permission from ref. 45. Copyright (2004) Elsevier.

surface is decorated with biomolecules. This configuration confers an extremely high F/P ratio on the AIE immunosensor.[45]

The nanocrystalline HPS biomarkers are used for sandwich-type immunoassays. The analyte is first immobilized by the capture antibody pre-adsorbed on a solid substrate and then exposed to the antibody-labeled bioprobe (step 4). The PL intensity increases with the analyte concentration (Fig. 23B).[45] The sensitivity of the HPS bioprobes is 140-fold higher than that of a fluorescein isothiocyanate (FITC)–antibody conjugate. The signals of the nanocrystalline bioprobes are dramatically amplified, thanks to the extremely high F/P ratios in the FIA system. This manifests the great value of the AIE effect to the development of ultrasensitive FIA systems.

Cationic AIE luminogens are turned on when encountering anionic biomacromolecules such as DNA and RNA due to electrostatic attraction-aided complexation or aggregation.[41,46] Linear relationships between the PL intensity and the analyte concentration have been identified, which facilitates nucleic acid analyses. We have recently observed specific recognition of DNA folding structures by a cationic TPE derivative named 1,1,2,2-tetrakis[4-(2-triethylammonioethoxy)phenyl]ethene tetrabromide (**41**).[47]

A single-stranded (ss) DNA with a guanine (G)-rich repeat sequence is known to fold into a secondary structure called a G-quadruplex. This structure is stabilized by monovalent cations (*e.g.*, K^+) located in the centers of the G-quadruplex plates. Quadruplex formation in human telomeric DNA can affect gene expression and inhibit telomerase activity in cancer cells. It is envisaged that the development of quadruplex-targeting drugs may enable artificial regulation of gene expression and control of cancel cell proliferation. The detection of the G-quadruplex structure thus has medicinal implications.

Because of its water miscibility, **41** is non-emissive in an aqueous buffer. When its molecules are bound to a DNA strand of HG21, the intramolecular rotation is restricted and the PL is thus turned on (Fig. 24, step 1). Addition of K^+ ions induces HG21 to fold into a G-quadruplex structure, resulting in a red shift (from 470 nm to 492 nm) in the PL spectrum (step 2). Hybridization with a complementary DNA (C21) unfolds the quadruplex and gives a duplex (ds) structure. The

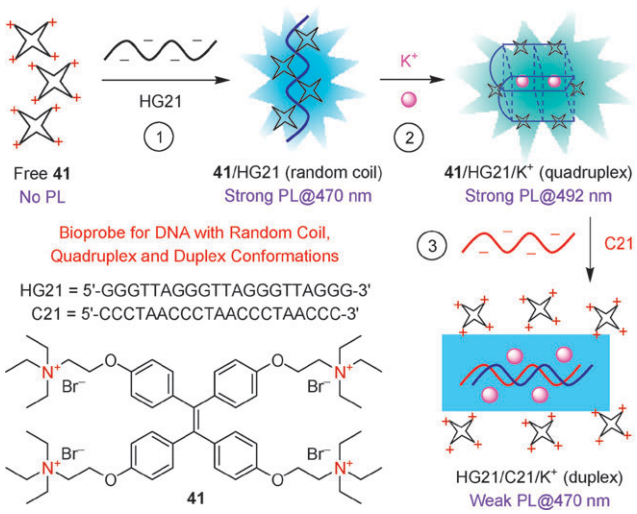

Fig. 24 PL of ammonium salt of TPE derivative **41** is turned on by binding to random coil of a DNA strand HG21 (step 1), red-shifted when complexed with G-quadruplex (step 2), and blue-shifted and weakened upon duplex formation with a complementary DNA strand C21 (step 3). Reproduced with permission from ref. 47. Copyright (2008) Wiley-VCH.

K^+ ions in the solution compete with the molecules of **41** to bind with the dsDNA structure. The overwhelmingly large quantity of K^+ ions helps them win the competition. As a result, the molecules of **41** are released back to the solution and its light emission is thus diminished (step 3).[47]

The spectral red shift diagnostically manifests the presence of a quadruplex structure, allowing a visual distinguishment of the G-quadruplex from other DNA conformations, especially the double helix structure. The distinct AIE characteristic of **41** enables real-time monitoring of the folding process of HG21 in the absence of any pre-attached luminogen labels on the DNA strand. These results are useful to biomedical investigations, especially to high-throughput quadruplex-targeting anticancer drug screening. Meanwhile, **41** can be used as a K^+ biosensor because of the high specificity of **41** for the K^+-stabilized G-quadruplex structure over those stabilized by other cationic species, such as Na^+, Li^+, NH_4^+, Mg^{2+} and Ca^{2+}.[47]

The PL turn-on switching of **41** on binding to an HG21 strand implies that the AIE luminogen can be used as a DNA marker in gel electrophoresis. After running a poly(acrylamide) gel electrophoresis (PAGE) of HG21, the gel plate is stained with a solution of **41** for 5 min. Upon UV illumination, the stained PAGE plate displays an emission band, whose brightness is increased with increasing HG21 concentration (Fig. 25A).[47] The control PAGE plates stained with ethidium bromide (EB), however, show no visible bands (Fig. 25B).

While EB is a widely used visualization agent in the PAGE assay, it takes at least 30 min to start to function.[5] Band visualization with EB is realized by its intercalation into the hydrophobic region of the DNA strands, which makes EB staining a slow process. On the other hand, the emission of **41** is activated by its spontaneous electrostatic interaction with the charged surfaces of DNA strands, which is therefore very fast.[47] A sensitivity test reveals that **41** can detect ~0.5 μM of

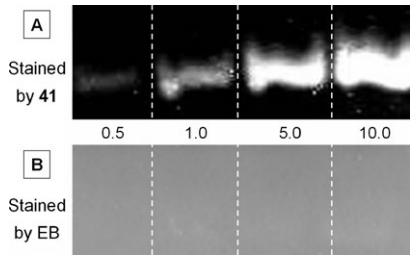

Fig. 25 Poly(acrylamide) gel electrophoresis (PAGE) assays of HG21 at concentrations of 0.5, 1.0, 5.0, and 10.0 μM. The gels were post-stained with 10 μM of (A) **41** and (B) ethidium bromide (EB) for 5 min. Adapted with permission from ref. 47. Copyright (2008) Wiley-VCH.

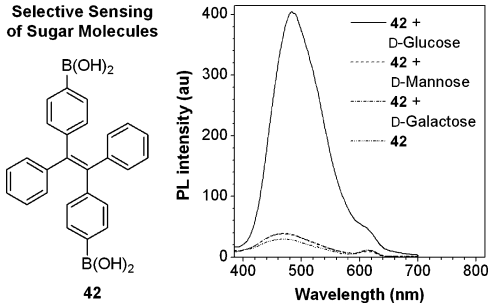

Fig. 26 PL spectra of aqueous solutions of TPE-bisboronic acid **42** in the absence and presence of D-glucose, D-galactose and D-mannose. Reproduced with permission from ref. 43*b*. Copyright (2009) Science in China Press.

HG21. The detection limit can be further lowered by increasing the concentration of the luminogen, owing to its AIE feature. Our visualization system thus has the advantages of fast response and high sensitivity, in addition to its excellent miscibility with aqueous media.

Sugars play important roles in biological processes such as metabolism. There is great demand for the development of convenient methods for selective recognition of sugars in aqueous media due to their obvious clinical and therapeutic values. For example, monitoring glucose levels in biological fluids such as urine and blood is essential for the management of diabetes.[48]

Boronic acids readily form boronate complexes with sugars in water.[49] Attaching boronic acid chelating groups to the phenyl rings of TPE yields **42**, a new AIE luminogen with two sugar-binding sites.[50] Adding D-glucose into a solution of **42** brings about a dramatic increase in the PL intensity, whereas little change in the PL spectrum is observed when D-mannose or D-galactose are used under identical conditions (Fig. 26). Specific conformation matching may be responsible for this selectivity for glucose over other monosaccharides.[51] As the two boronic acid chelators of **42** cannot bind to one glucose molecule due to the involved steric effect, the 1 : 1 complexation of **42** with glucose may have resulted in the formation of oligoboronates. The oligomeric chains may fold and aggregate in the aqueous medium, thus making **42** a glucose-selective light-up probe.

Amphiphilic biomolecules such as phospholipids assemble into well-organized nanostructures such as micellar aggregates under appropriate conditions.[5] Evaluation of the critical micelle concentration (CMC) is very important but has not been easy at all. Whilst osmotic pressure, equivalent conductivity, and interfacial tension have been used to measure CMCs, none of them is handy. We used lecithin as a model biomolecule to check whether an AIE luminogen could act as a simple beacon for CMC determination.[43]

When the concentration of lecithin is low, it is molecularly dissolved. Molecules of $\mathbf{39}^{2+}$ are also genuinely dissolved in acidic media[40] and the solution is thus non-emissive (Fig. 27). The solution becomes emissive when large amounts of lecithin are present in the solution of $\mathbf{39}^{2+}$. Plotting the PL intensity against the lecithin concentration gives two lines that intersect at a specific concentration, which is the CMC for the micellar system. At the CMC, the lecithin molecules start to form micellar nanoaggregates. The molecules of $\mathbf{39}^{2+}$ enter the micelles to aggregate and hence emit, thanks to its AIE nature. The AIE luminogen thus functions as a handy nanoaggregate beacon for CMC evaluation, as can be visually appreciated from the photographs shown in Fig. 27.[43]

Biocompatibility is the key factor that determines whether a bioprobe can be used for *in vivo* applications. To be a useful cell tracer, a luminogen should neither inhibit nor promote the growth of living cells. The cytotoxicity of **43** has been tested in dimethyl sulfoxide (DMSO) solutions with a DMSO content of $<0.1\%$, as DMSO exerts no biological effect on cell proliferation when its amount in the medium is $<0.2\%$.[5] In the presence of **43**, HeLa cells grow as normal as they do in the control experiment (Fig. 28).[52] Evidently, **43** is nontoxic to the living cells. In other words, it is cytocompatible without interfering with the metabolism of living cells.

The excellent biocompatibility of **43** prompted us to utilize it for intracellular imaging. When HeLa cells are stained with nanoaggregates of **43**, the cells are clearly imaged in an exposure time as short as 1 s (Fig. 29A).[52] Under identical imaging conditions, commercial fluorescent dye CellTracker™ Green CMFDA shows an inferior performance: the images of the cells can hardly been seen when the stained HeLa cells are exposed for 1 s (Fig. 29B). Clear images can finally be taken when the exposure time is prolonged to 5 s.

Closer inspection of the fluorescence images reveals that the nanoaggregates of **43** stain the cytoplasmic regions of the cells

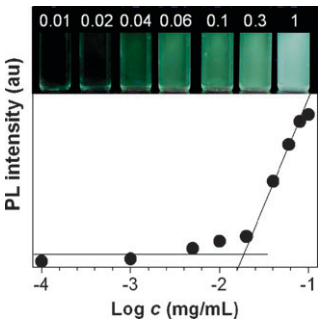

Fig. 27 Plot of PL intensity of $\mathbf{39}^{2+}$ *versus* concentration of lecithin (*c*) in an acidic aqueous medium (pH = 3). Photographs of the solutions were taken under illumination of a UV lamp. Reproduced with permission from ref. 43*b*. Copyright (2009) Science in China Press.

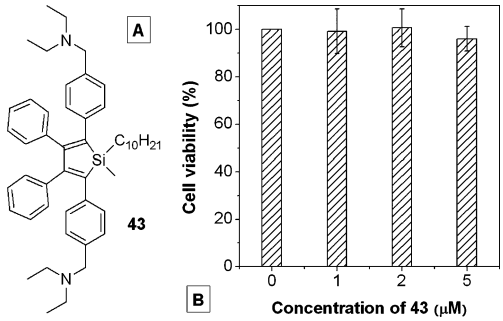

Fig. 28 (A) Chemical structure of diaminated silole derivative **43** and (B) its effect on the viability of living HeLa cells evaluated by MTT assay. MTT = 3-(4,5-dimethyl-2-thiazolyl)-2,5-diphenyltetrazolium bromide. Reproduced with permission from ref. 52. Copyright (2009) Science in China Press.

but the CMFDA molecules stain the entire cells. This is probably because the former is hydrophobic but the latter is hydrophilic. Water-soluble fluorophores such as CMFDA can pass through membranes to enter the cells. The small CMFDA molecules can also enter the nucleus through nuclear pores. The fluorophore therefore can label both the cytoplasmic and nuclear compartments of the living cells (Fig. 29C).

The major route for the nanoaggregates of **43** to enter a cell is through endocytosis. During this process, the aggregates are enclosed by the cell membrane to form small vesicles that can be internalized by the cell. Inside the cell, the nanoaggregates can be further processed in endosomes and lysosomes and are eventually released from the cellular organelles. However, the hydrophobic nature of the nanoaggregates prevents them from entering the nucleus of the cell. When the nanoaggregates are bound to the biopolymers in the cytoplasm, they become very luminescent, due to the additional physical restriction of their intramolecular rotation.

The fact that the nanoaggregates of **43** selectively stain the cytoplasmic regions of the cells gives this AIE luminogen a unique advantage over the CellTracker that stains the whole cells. In most cases of cell imaging, it is necessary to use two different fluorogens to stain a cell: one to stain DNA in the nucleus, and another to stain the cytoplasm. Our AIE dye is thus a better choice when used in combination with a DNA-staining luminogen.

Miscellaneous systems

As described above, nanoaggregates of AIE luminogens suspended in aqueous mixtures can be used as fluorescent chemosensors. We proceeded further to develop solid-state detection strips for chemical species such as metallic ions in water, which may find applications in water quality control, pollution tracing and environmental protection. Employing an electrospinning technique, composite films are prepared from blends of HPS and PMMA. Macroscopically, the thin films look uniform but microscopically they are found to contain many microspheres and nanofibers (Fig. 30A).[53] There exist many nanosized pores and protuberances in the microspheres. This distinct structure resembles that of a lotus leaf surface.[54] The contact angle (CA) of a water droplet on the HPS/PMMA micro/nanocomposite film is 115 ± 2.6°, indicating that the film surface is very hydrophobic (Fig. 30A, inset).

In pure water, the film emits a strong blue green light at 481 nm (Fig. 30B). This emission is quenched when the film is immersed in an aqueous ferric solution, giving a K_{sv} value of 6.21×10^3 M^{-1}.[53] The Fe^{3+} ions can be washed away by placing the film in pure water, thanks to its lotus-like structure and high hydrophobicity. By alternatively putting the film in pure water and ferric solution, the emission can be repeatedly and reversibly switched between bright and dark states with excellent reproducibility for many cycles (Fig. 30B, inset).[53]

Fabrication of nanowires has attracted much interest owing to their unique material properties and enormous application potentials.[25c,55] Nanowires of HPS can be facilely prepared by using an anodic aluminium oxide (AAO) membrane as a template. Examples of HPS nanowires with average diameters of 70 and 150 nm are shown in panels A and B of Fig. 31, respectively. The nanowires are aligned in a continuous, parallel manner with an average length of *ca.* 60 μm. The nanowires are highly luminescent due to the AIE properties of the silole aggregates. Intriguingly, the emission peak bathochromically shifts with an increase in the nanowire diameter (Fig. 31C).[55a]

In our early studies, we have observed that the emissions of AIE aggregates bathochromically shift when they undergo a morphology change from the crystalline to the amorphous

Fig. 29 Fluorescence images of living HeLa cells stained with (A) **43** and (B, C) CellTracker™ Green CMFDA. Exposure time: (A, B) 1 s, (C) 5 s. Reproduced with permission from ref. 52. Copyright (2009) Science in China Press.

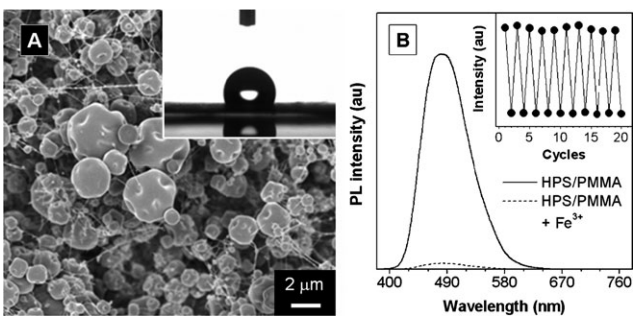

Fig. 30 (A) SEM image of an electrospun HPS/PMMA composite film. Inset: photograph of the shape of a water droplet on the film with a contact angle of 115 ± 2.6°. (B) PL spectra of the electrospun film in pure water (HPS/PMMA) and in an aqueous Fe^{3+} solution (HPS/PMMA + Fe^{3+}). Inset: reversible switching between emissive and non-emissive states by immersing the HPS/PMMA film in pure water and an Fe^{3+} solution, respectively. Reproduced with permission from ref. 53. Copyright (2008) Wiley-VCH.

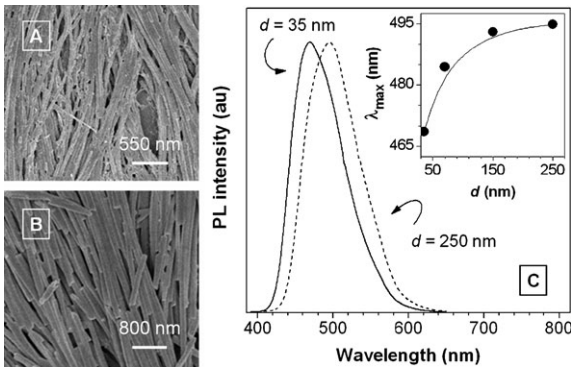

Fig. 31 SEM images of HPS nanowires with average diameters (*d*) of (A) 70 and (B) 150 nm. (C) PL spectra of HPS nanowires with average diameters of 35 and 250 nm. Inset: plot of emission maximum (λ_{max}) *versus* nanowire diameter (*d*). Reproduced with permission from ref. 55*a*. Copyright (2007) Wiley-VCH.

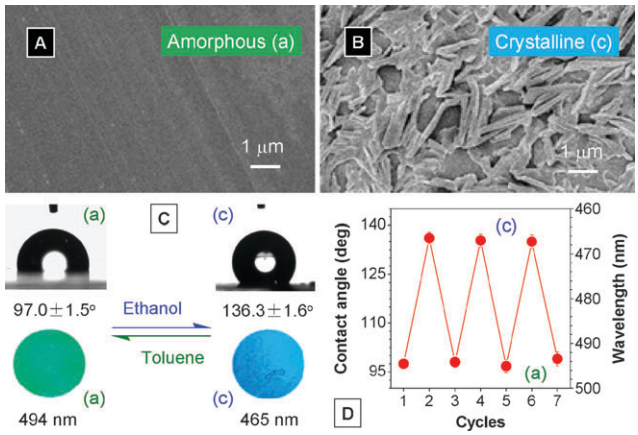

Fig. 32 (A) Amorphous and (B) crystalline films of HPS. (C) Shapes of water droplets on, and colours of light emissions from, the amorphous and crystalline films of HPS. (D) Reversible switching of contact angle and emission colour of HPS by repeatedly exposing its amorphous and crystalline films to ethanol and toluene vapours, respectively. Reproduced with permission from ref. 56. Copyright (2008) American Chemical Society.

state (*vide ante*). Crystals of HPS, for example, emit a blue light of ~465 nm, while its amorphous powders emit a green light of ~490 nm. The emission peak of the "thin" HPS nanowires (d = 35 nm) is close to that of the HPS crystals, suggesting that these nanowires are crystalline in morphology. On the other hand, the "thick" nanowires (d = 250 nm) emit at 495 nm, close to that of the HPS powders (Fig. 31C). This indicates that the red shift in the emission peak with increasing nanowire size stems from the crystalline to amorphous phase transition.

In the nanowire fabrication process, the nanopores in the AAO template are filled with saturated HPS solution due to capillary action. The saturated vapor tension in the small channels (*e.g.*, 35 nm) is high, which slows down the solvent evaporation process. This gives the HPS molecules enough time to reorient and crystallize. As the diameter of the AAO channel is increased, the saturated vapor tension is decreased. This accelerates the solvent evaporation, giving no time for the HPS molecules to pack regularly so they agglomerate abruptly. Amorphous nanowires are thus formed in the AAO channels with large diameters. Evidently, the PL of the nanowires can be tuned by changing their morphologies, which are realized by simply varying the channel sizes of the AAO template.

"Smart" or "intelligent" materials change their properties in response to external stimuli or perturbations. Most existing stimuli-responsive smart materials change a single property in a "one-way" fashion. Research into "two-way" intelligent materials, *i.e.*, those capable of reversibly switching between two properties, is still in its infancy. We have developed a dual-responsive system based on HPS.[56] The film prepared by spin-coating is smooth and featureless (Fig. 32A), suggesting that the film is amorphous. Fuming the film with ethanol vapour induces the HPS molecules to reorient, giving a crystalline film full of fine structures of nanosheets and nanorods (Fig. 32B). This morphological change is reversible: the crystalline film can be transformed to the amorphous one by exposing it to toluene vapour (Fig. 32C).

The surface wettability of the thin films is evaluated by CA measurement. The CA of the amorphous film is 97.0 ± 1.5°, indicating that its surface is hydrophobic. After controlled fumigation with ethanol vapour, the water droplet shrinks to a CA value of 136.3 ± 1.6°, meaning that the film becomes more hydrophobic (Fig. 32C). The crystalline film is changed to amorphous one when fumed with toluene vapour, accompanied by a drop in the CA value (from 136° to 97°) and a shift in the PL color (from blue to green). The changes in the surface wettability and solid-state emission can be repeated many times without fatigue, indicative of an excellent reversibility of the two-way switching processes (Fig. 32D).[56]

The AIE luminogens are highly emissive in the solid state, making them ideal candidate materials for the fabrication of efficient OLEDs. Using the AIE luminogens as light-emitting layers, multilayer OLEDs can be fabricated.[15*b*,21,31*c*,57] An OLED with a configuration of ITO/CuPc/TPD/MPPS/Mg–Ag[58] emits a green light of 496 nm. When an AlQ_3 layer is introduced, the device of ITO/CuPc/TPD/MPPS/AlQ_3/LiF–Al is turned on at 3.4 V (Table 2, no. 1).[59] The OLED produces a maximum luminance of 9234 cd m^{-2}, a maximum current efficiency of 20 cd A^{-1} and a power efficiency of 14 lm W^{-1}. Its external quantum efficiency is 8%, well approaching the limit of that possible in the electroluminescence (EL) devices based on organic singlet emitters.[59]

Similarly impressive device performance is shown by the OLED of HPS (Table 2, no. 2). Its maximum luminance is remarkably high (55 880 cd m^{-2}). The OLED of diphenylated TPE derivative **17** also emits brilliantly, giving a maximum brightness of 10 680 cd m^{-2}.[31*c*] Although the device structures are yet to be optimized, these performance data already make them hopeful for finding applications in, for example, flat-panel lighting and displays. Whereas researchers in the area are trying hard to avoid crystal formation in the device fabrication processes, the crystalline layers made of the AIE luminogens offer excellent device performances due to the high charge mobility in the crystals.[57] This feature distinguishes our AIE luminogens from the conventional

Table 2 Performances of OLED devices [a] based on AIE emitters[59,31c]

No.	Emitter	V_{on}	λ_{max}	CE	PE	L	η_{EL}
1	MPPS (**2**)	3.4	510	20	14	9234	8
2	HPS (**1**)	4.0	490	25	10	55 880	7
3	**17**	5.0	476	5.2	9	10 680	2.6

[a] For OLED device configurations, see ref. 15*b*, 21, 31*c* and 57–59. Abbreviations: V_{on} = turn-on voltage (V), λ_{max} = emission maximum (nm), CE = maximum current efficiency (cd A^{-1}), PE = maximum power efficiency (lm W^{-1}), L = maximum luminance (cd m^{-2}), and η_{EL} = external electroluminescence quantum efficiency (%).

fluorophores and promises the development of OLEDs with high efficiencies.

Concluding remarks

In this work, we have discovered a novel AIE phenomenon: molecules non-luminescent in solutions are induced to emit by aggregate formation. We have proposed that the RIR process accounts for the AIE effect and designed a series of control experiments to validate our hypothesis. On the basis of our mechanistic understanding, we have developed a large variety of new fluorescent and phosphorescent AIE luminogens with emission colours covering the entire visible spectral region and luminescence efficiencies up to unity. This in turn proves that the AIE effect is a general property for propeller-like molecules consisting of π-conjugated rotors and stators. We have explored the potential applications of AIE luminogens as chemical sensors, biological probes, smart nanomaterials, and solid-state emitters.

Traditional luminophores are usually flat disk-like aromatic molecules, which experience strong molecular interactions in concentrated solutions and solid aggregates. This leads to early observations and the eventual evolution into the general belief that concentration quenching is "common to most aromatic hydrocarbons and their derivatives".[2] Luminophore aggregation has almost always been linked with the ACQ effect. In this work, we clear the name of aggregation and prove that it can work to our benefit through judicious structural design or molecular engineering.

The dynamic molecular motion, such as the intramolecular rotation, of propeller-like molecules effectively consumes the energy of their excited states and makes them non-emissive in solution. These molecules are likely to be eliminated in the early stages of the screening process for candidate emitters for the fabrication of OLEDs because the photophysical property evaluations have traditionally been done in dilute solutions. It has been a common "law" that a poor emitter in the solution state will not luminesce efficiently in the solid state. Our work proves that this is not necessarily true. It teaches us to not prematurely discard a molecule non-emissive in the solution state because the molecule could be highly luminescent in the aggregated state. This evidently helps widen our search avenue for efficient light emitters in the solid state.

Nonplanar molecules can hardly pack in a face-to-face manner and therefore experience little π–π stacking interaction when they aggregate. The emissions of these molecules are not quenched by aggregation because excimers/exciplexes are difficult to form in their aggregates. Aggregate formation, on the other hand, rigidifies their molecular conformations and activates the RIR process, thus making the molecules emissive in the solid state. The CIP effect is observed in the organic crystals, owing to the severe restrictions on the molecular rotation imposed by the crystalline lattice. This is remarkable because pure organic phosphors have been rare species.

The AIE effect permits the use of concentrated solutions of luminogens and their aggregate suspensions in aqueous media for sensing applications. In comparison to the turn-off sensors based on the ACQ effect of dilute solutions of conventional luminophores, the AIE solutions and suspensions are more emissive and sensitive and photobleaching-resistant. The turn-on/light-up nature of the AIE sensors makes them promising for field trials, on-site screening, household testing, *etc*. The AIE aggregates can be directly used without any protection of their surfaces and are therefore superior to their inorganic QD counterparts, thanks to the excellent biocompatibility of the organic aggregates.

To fabricate efficient OLEDs, scientists have worked hard to hamper crystal formation and to prepare amorphous solid films, because luminophore crystallization is known to quench light emission, although charge transport in a crystalline film is faster than in an amorphous film. The CIE and CIP effects of AIE crystals are particularly helpful for the development of efficient EL devices, as demonstrated by the outstanding device performances of the OLEDs constructed from the AIE luminogens.[57–59]

We now know that the AIE effect is caused mainly by the RIR process. This process actually also plays an important role in bioluminescence systems. For example, *trans*-stilbene is only weakly luminescent in solution, owing to non-radiative decay of its excited state *via cis–trans* rotational isomerization. However, the antibody elicited against *trans*-stilbene emits efficiently, due to the complex formation in a ligand-binding pocket in the rigid protein matrix.[60] Similarly, emission of the chromophore in a denatured green fluorescent protein (GFP) is quenched in solution due to the free intramolecular rotation. In the native GFP, the chromophore is covalently bound to the middle of an internal α-helix directed along a rigid β-barrel axis. This provides steric hindrance to the *cis–trans* rotational isomerization and confers superb fluorescence properties on the protein.[61] Given the importance of the RIR process in bioluminescence systems,[60,61] the bioprobe applications of AIE dyes demonstrated in this article is thus just a beginning, with many more possibilities waiting to be explored.

As a final remark, we wish to point out that a large amount of outstanding work has been done by many other research groups in the area of AIE research over the past years, with full-colour emissions in efficiencies up to unity accomplished. The length limitation to a short account has forced us to focus on our own AIE work and interested readers are encouraged to read the papers published by other groups, some examples of which are given in the reference section of this article.[13,14,62] The AIE effect offers a new platform for the study of solid-state luminescence processes. We are enthusiastically looking forward to new advancements in this exciting area of research.

Acknowledgements

This work was partially supported by the Research Grants Council of Hong Kong, the National Basic Research Program of the Ministry of Science and Technology of China, and the National Science Foundation of China. We acknowledge the contributions from our collaborators, whose names are given in the references section. B. Z. T. thanks the Cao Guangbiao Foundation of Zhejiang University for support.

Notes and references

1 Th. Förster and K. Kasper, *Z. Phys. Chem. (Munich)*, 1954, **1**, 275.

2 J. B. Birks, *Photophysics of Aromatic Molecules*, Wiley, London, 1970.

3 (*a*) J. Malkin, *Photophysical and Photochemical Properties of Aromatic Compounds*, CRC, Boca Raton, 1992; (*b*) N. J. Turro, *Modern Molecular Photochemistry*, University Science Books, Mill Valley, 1991; (*c*) X.-C. Li and S. C. Moratti, in *Photonic Polymer Systems*, ed. D. L. Wise, G. E. Wnek, D. J. Trantolo, T. M. Cooper and J. D. Gresser, Marcel Dekker, New York, 1998, ch. 10.

4 (*a*) J. Slavík, *Fluorescence Microscopy and Fluorescent Probes*, Plenum, New York, 1996; (*b*) B. Valeur, *Molecular Fluorescence: Principle and Applications*, Wiley-VCH, Weinheim, 2002.

5 (*a*) *Advanced Concepts in Fluorescence Sensing*, ed. C. D. Geddes and J. R. Lakopwicz, Springer, Norwell, 2005; (*b*) *Fluorescence Sensors and Biosensors*, ed. R. B. Thompson, CRC, Boca Raton, 2006; (*c*) W. H. Tan, K. M. Wang and T. J. Drake, *Curr. Opin. Chem. Biol.*, 2004, **8**, 547; (*d*) K. E. Sapsford, L. Berti and I. L. Medintz, *Angew. Chem., Int. Ed.*, 2006, **45**, 4562; (*e*) S. M. Borisov and O. S. Wolfbeis, *Chem. Rev.*, 2008, **108**, 423.

6 (*a*) A. P. Alivisatos, W. Gu and C. Larabell, *Annu. Rev. Biomed. Eng.*, 2005, **7**, 55; (*b*) I. L. Medintz, H. T. Uyeda, E. R. Goldman and H. Mattoussi, *Nat. Mater.*, 2005, **4**, 435; (*c*) M. De, P. S. Ghosh and V. M. Rotello, *Adv. Mater.*, 2008, **20**, 4225.

7 (*a*) D. W. Domaille, E. L. Que and C. J. Chang, *Nat. Chem. Biol.*, 2008, **4**, 168; (*b*) M. H. Lim and S. J. Lippard, *Acc. Chem. Res.*, 2007, **40**, 41; (*c*) B. N. G. Giepmans, S. R. Adams, M. H. Ellisman and R. Y. Tsien, *Science*, 2006, **312**, 217; (*d*) E. A. Jares-Erijman and T. M. Jovin, *Nat. Biotechnol.*, 2003, **21**, 1387.

8 (*a*) S. W. Thomas III, G. D. Joly and T. M. Swager, *Chem. Rev.*, 2007, **107**, 1339; (*b*) M. Belletête, J. Bouchard, M. Leclerc and G. Durocher, *Macromolecules*, 2005, **38**, 880; (*c*) A. Menon, M. Galvin, K. A. Walz and L. Rothberg, *Synth. Met.*, 2004, **141**, 197; (*d*) C.-T. Chen, *Chem. Mater.*, 2004, **16**, 4389; (*e*) M. Grell, D. D. C. Bradley, G. Ungar, J. Hill and K. S. Whitehead, *Macromolecules*, 1999, **32**, 5810; (*f*) R. Jakubiak, C. J. Collison, W. C. Wan and L. Rothberg, *J. Phys. Chem. A*, 1999, **103**, 2394; (*g*) M. Grell, D. D. C. Bradley, X. Long, T. Chamberlain, M. Inbasekaran, E. P. Woo and M. Soliman, *Acta Polym.*, 1998, **49**, 439; (*h*) U. Lemmer, S. Heun, R. F. Mahrt, U. Scherf, M. Hopmeier, U. Siegner, E. O. Gobel, K. Müllen and H. Bassler, *Chem. Phys. Lett.*, 1995, **240**, 373.

9 (*a*) A. C. Grimsdale and K. Müllen, *Adv. Polym. Sci.*, 2008, **212**, 1; (*b*) W. W. H. Wong and A. B. Holmes, *Adv. Polym. Sci.*, 2008, **212**, 85; (*c*) P. L. T. Boudreault, N. Blouin and M. Leclerc, *Adv. Polym. Sci.*, 2008, **212**, 99; (*d*) J. C. Sanchez and W. C. Trogler, *Macromol. Chem. Phys.*, 2008, **209**, 1527; (*e*) Y. Zhang, B. Liu and Y. Cao, *Chem.–Asian J.*, 2008, **3**, 739; (*f*) J. Chen and Y. Cao, *Macromol. Rapid Commun.*, 2007, **28**, 1714; (*g*) V. W. W. Yam and K. M. C. Wong, *Top. Curr. Chem.*, 2005, **257**, 1; (*h*) F. J. M. Hoeben, P. Jonkheijm, E. W. Meijer and A. P. H. J. Schenning, *Chem. Rev.*, 2005, **105**, 1491; (*i*) W. Lu, M. C. W. Chan, N. Y. Zhu, C. M. Che, Z. He and K. Y. Wong, *Chem.–Eur. J.*, 2003, **9**, 6155; (*j*) U. H. F. Bunz, *Chem. Rev.*, 2000, **100**, 1605; (*k*) F. Hide, M. A. Diaz-Garcia, B. J. Schwartz and A. J. Heeger, *Acc. Chem. Res.*, 1997, **30**, 430.

10 (*a*) C. W. Tang and S. A. Vanslyke, *Appl. Phys. Lett.*, 1987, **51**, 913; (*b*) J. H. Burroughes, D. D. C. Bradley, A. R. Brown, R. N. Marks, K. Mackay, R. H. Friend, P. L. Burns and A. B. Holmes, *Nature*, 1990, **347**, 539; (*c*) T. Y. Luh, S. Basu and R. N. Chen, *Curr. Sci.*, 2000, **78**, 1352; (*d*) A. P. Kulkarni, C. J. Tonzola, A. Babel and S. A. Jenekhe, *Chem. Mater.*, 2004, **16**, 4556; (*e*) B. W. D'Andrade and S. R. Forrest, *Adv. Mater.*, 2004, **16**, 1585.

11 (*a*) J.-S. Yang and J.-L. Yan, *Chem. Commun.*, 2008, 1501; (*b*) Y.-T. Lee, C.-L. Chiang and C.-T. Chen, *Chem. Commun.*, 2008, 217; (*c*) J. Wang, Zhao, Y. C. Dou, H. Sun, P. Xu, K. Ye, J. Zhang, S. Jiang, F. Li and Y. Wang, *J. Phys. Chem. B*, 2007, **111**, 5082; (*d*) C.-W. Wu, C.-M. Tsai and H.-C. Lin, *Macromolecules*, 2006, **39**, 4298; (*e*) S.-F. Lim, R. H. Friend, I. D. Rees, J. Li, Y. Ma, K. Robinson, A. B. Holms, E. Hennebicq, D. Beljonne and F. Cacialli, *Adv. Funct. Mater.*, 2005, **15**, 981; (*f*) F. He, Y. Tang, S. Wang, Y. Li and D. Zhu, *J. Am. Chem. Soc.*, 2005, **127**, 12343; (*g*) C. Fan, S. Wang, J. W. Hong, G. C. Bazan, K. W. Plaxco and A. J. Heeger, *Proc. Natl. Acad. Sci. U. S. A.*, 2003, **100**, 6297; (*h*) S. Setayesh, A. C. Grimsdale, T. Weil, V. Enkelmann, K. Müllen, F. Meghdadi, E. J. W. List and G. Leising, *J. Am. Chem. Soc.*, 2001, **123**, 946; (*i*) S. Hecht and J. M. J. Frechet, *Angew. Chem., Int. Ed.*, 2001, **40**, 74; (*j*) R. Jakubiak, Z. Bao and L. Rothberg, *Synth. Met.*, 2000, **114**, 61; (*k*) A. Kraft, A. C. Grimsdale and A. B. Holmes, *Angew. Chem., Int. Ed.*, 1998, **37**, 402.

12 (*a*) B. T. Nguyen, J. E. Gautrot, C. Ji, P.-L. Brunner, M. T. Nguyen and X. X. Zhu, *Langmuir*, 2006, **22**, 4799; (*b*) A. P. Kulkarni and S. A. Jenekhe, *Macromolecules*, 2003, **36**, 5285; (*c*) S. Abe and L. Chen, *J. Polym. Sci., Part B: Polym. Phys.*, 2003, **41**, 1676; (*d*) B. S. Gaylord, S. Wang, A. J. Heeger and G. C. Bazan, *J. Am. Chem. Soc.*, 2001, **123**, 6417; (*e*) L. Chen, S. Xu, D. McBranch and D. Whitten, *J. Am. Chem. Soc.*, 2000, **122**, 9302; (*f*) P. N. Taylor, M. J. O'Connell, L. A. McNeill, M. J. Hall, R. T. Aplin and H. L. Anderson, *Angew. Chem., Int. Ed.*, 2000, **39**, 3456; (*g*) D. Sainova, T. Miteva, G. Nothofer, U. Scherf, I. Glowacki, J. Ulanski, H. Fujikawa and D. Neher, *Appl. Phys. Lett.*, 2000, **76**, 1810.

13 (*a*) K. Kokado and Y. Chujo, *Macromolecules*, 2009, **42**, 1418; (*b*) J. Dong, K. M. Solntsev and L. M. Tolbert, *J. Am. Chem. Soc.*, 2009, **131**, 662; (*c*) W. Tang, Y. Xiang and A. Tong, *J. Org. Chem.*, 2009, **74**, 2163; (*d*) H. Yao, M. Yamashita and K. Kimura, *Langmuir*, 2009, **25**, 1131; (*e*) K.-Y. Pu and B. Liu, *Adv. Funct. Mater.*, 2009, **19**, 277; (*f*) M. Wang, D. Zhang, G. Zhang and D. Zhu, *Chem. Commun.*, 2008, 4469; (*g*) J. Lv, L. Jiang, C. Li, X. Liu, M. Yuan, J. Xu, W. Zhou, Y. Song, H. Liu, Y. Li and D. Zhu, *Langmuir*, 2008, **24**, 8297; (*h*) Y. Liu, X. Tao, F. Wang, X. Dang, D. Zou, Y. Ren and M. Jiang, *J. Phys. Chem. C*, 2008, **112**, 3975; (*i*) R. Davis, N. S. S. Kumar, S. Abraham, C. H. Suresh, N. P. Rath, N. Tamaoki and S. Das, *J. Phys. Chem. C*, 2008, **112**, 2137; (*j*) Q. Zhao, L. Li, F. Li, N. Yu, Z. Liu, T. Yi and C. Huang, *Chem. Commun.*, 2008, 685; (*k*) Z. Ning, Z. Chen, Q. Zhang, Y. Yan, S. Qian, Y. Cao and H. Tian, *Adv. Funct. Mater.*, 2007, **17**, 3799; (*l*) D. Yan, J. Mohsseni-Ala, N. Auner, M. Bolte and J. W. Bats, *Chem.–Eur. J.*, 2007, **13**, 7204; (*m*) Y. Qian, S. Li, G. Zhang, Q. Wang, S. Wang, H. Xu, C. Li, Y. Li and G. Yang, *J. Phys. Chem. B*, 2007, **111**, 5861; (*n*) S. Kim, T. Y. Ohulchanskyy, H. E. Pudavar, R. K. Pandey and P. N. Prasad, *J. Am. Chem. Soc.*, 2007, **129**, 2669; (*o*) Y. Li, F. Li, H. Zhang, Z. Xie, W. Xie, H. Xu, B. Li, F. Shen, L. Ye, M. Hanif, D. Ma and Y. Ma, *Chem. Commun.*, 2007, 231.

14 (*a*) L. Qian, J. Zhi, B. Tong, F. Yang, W. Zhao and Y. Dong, *Prog. Chem. (Beijing, China)*, 2008, **20**, 673; (*b*) T. Baumgartner and R. Reau, *Chem. Rev.*, 2006, **106**, 4681; (*c*) C. J. Bhongale and C. S. Hsu, *Angew. Chem., Int. Ed.*, 2006, **45**, 1404; (*d*) Y. Sun, J. Liao, J. Fang, P. Chou, C. Shen, C. Hsu and L. Chen, *Org. Lett.*, 2006, **8**, 3713; (*e*) C. Bao, R. Lu, M. Jin, P. Xue, C. Tan, T. Xu, G. Liu and Y. Zhao, *Chem.–Eur. J.*, 2006, **12**, 3287; (*f*) Z. Wang, H. Shao, J. Ye, L. Tang and L. Lu, *J. Phys. Chem. B*, 2005, **109**, 19627; (*g*) S. J. Toal, D. Magde and W. C. Trogler, *Chem. Commun.*, 2005, 5465; (*h*) M. Han and M. Hara, *J. Am. Chem. Soc.*, 2005, **127**, 10951; (*i*) C. J. Bhongale, C. W. Chang, C. S. Lee, E. W. G. Diau and C. S. Hsu, *J. Phys. Chem. B*, 2005, **109**, 13472; (*j*) S. Jayanty and T. P. Radhakrishnan, *Chem.–Eur. J.*, 2004, **10**, 791; (*k*) S. Y. Ryu, S. Kim, J. Seo, Y. W. Kim, O. H. Kwon, D. J. Jang and S. Y. Park, *Chem. Commun.*, 2004, 70; (*l*) H. C. Yeh, S. J. Yeh and C. T. Chen, *Chem. Commun.*, 2003, 2632; (*m*) B. K. An, S. K. Kwon, S. D. Jung and S. Y. Park, *J. Am. Chem. Soc.*, 2002, **124**, 14410; (*n*) C. Belton, D. F. O'Brien,

W. J. Blau, A. J. Cadby, P. A. Lane, D. D. C. Bradley, H. J. Byrne, R. Stockmann and H. H. Horhold, *Appl. Phys. Lett.*, 2001, **78**, 1059; (*o*) L. Antolini, E. Tedesco, G. Barbarella, L. Favaretto, G. Sotgiu, M. Zambianchi, D. Casarini, G. Gigli and R. Cingolani, *J. Am. Chem. Soc.*, 2000, **122**, 9006; (*p*) R. Deans, J. Kim, M. R. Machacek and T. M. Swager, *J. Am. Chem. Soc.*, 2000, **122**, 8565.

15 (*a*) J. Luo, Z. Xie, J. W. Y. Lam, L. Cheng, H. Chen, C. Qiu, H. S. Kwok, X. Zhan, Y. Liu, D. Zhu and B. Z. Tang, *Chem. Commun.*, 2001, 1740; (*b*) B. Z. Tang, X. Zhan, G. Yu, P. P. S. Lee, Y. Liu and D. Zhu, *J. Mater. Chem.*, 2001, **11**, 2974.

16 M. Freemantle, *Chem. Eng. News*, 2001, **79**, 29.

17 (*a*) J. W. Y. Lam and B. Z. Tang, *Acc. Chem. Res.*, 2005, **38**, 745; (*b*) J. W. Y. Lam and B. Z. Tang, *J. Polym. Sci., Part A: Polym. Chem.*, 2003, **41**, 2607; (*c*) B. Z. Tang, *Polym. News*, 2001, **26**, 262.

18 (*a*) B. Z. Tang, *Macromol. Chem. Phys.*, 2008, **209**, 1303; (*b*) M. Häußler and B. Z. Tang, *Adv. Polym. Sci.*, 2007, **209**, 1.

19 (*a*) K. Tamao and S. Yamaguchi, *J. Organomet. Chem.*, 2000, **611**, 500; (*b*) M. M Sartin, A. J. Boydston, B. L. Pagenkopf and A. J. Bard, *J. Am. Chem. Soc.*, 2006, **128**, 10163; (*c*) J. Ohshita, K. H. Lee, K. Kimura and A. Kunai, *Organometallics*, 2004, **23**, 5622.

20 J. Chen, C. C. W. Law, J. W. Y. Lam, Y. Dong, S. M. F. Lo, I. D. Williams, D. Zhu and B. Z. Tang, *Chem. Mater.*, 2003, **15**, 1535.

21 G. Yu, S. Yin, Y. Liu, J. Chen, X. Xu, X. Sun, D. Ma, X. Zhan, Q. Peng, Z. Shuai, B. Z. Tang, D. Zhu, W. Fang and Y. Luo, *J. Am. Chem. Soc.*, 2005, **127**, 6335.

22 B. Z. Tang, Y. Geng, J. W. Y. Lam, B. Li, X. Jing, X. Wang, F. Wang, A. B. Pakhomov and X. Zhang, *Chem. Mater.*, 1999, **11**, 1581.

23 X. Fan, J. Sun, F. Wang, Z. Chu, P. Wang, Y. Dong, R. Hu, B. Z. Tang and D. Zou, *Chem. Commun.*, 2008, 2989.

24 (*a*) L. He, F. Xiong, S. Li, Q. Gan, G. Zhang, Y. Li, B. Zhang, B. Chen and G. Yang, *J. Phys. Chem. B*, 2004, **108**, 7092; (*b*) S. Li, Q. Wang, Y. Qian, S. Wang, Y. Li and G. Yang, *J. Phys. Chem. A*, 2007, **111**, 11793.

25 (*a*) M. H. Lee, D. Kim, J. W. Y. Lam and B. Z. Tang, *J. Korean Phys. Soc.*, 2004, **45**, 329; (*b*) Y. Ren, J. W. Y. Lam, Y. Dong, B. Z. Tang and K. S. Wong, *J. Phys. Chem. B*, 2005, **109**, 1135; (*c*) Y. Ren, Y. Dong, J. W. Y. Lam, B. Z. Tang and K. S. Wong, *Chem. Phys. Lett.*, 2005, **402**, 468; (*d*) C. J. Bhongale, C. W. Chang, E. W. G. Diau, C. S. Hsu, Y. Dong and B. Z. Tang, *Chem. Phys. Lett.*, 2006, **419**, 444.

26 (*a*) Q. Peng, Y. Yi, Z. Shuai and J. Shao, *J. Am. Chem. Soc.*, 2007, **129**, 9333; (*b*) S. Yin, Q. Peng, Z. Shuai, W. Fang, Y. H. Wang and Y. Luo, *Phys. Rev. B: Condens. Matter Mater. Phys.*, 2006, **73**, 205409.

27 Z. Li, Y. Dong, B. Mi, Y. Tang, M. Haeussler, H. Tong, Y. Dong, J. W. Y. Lam, Y. Ren, H. H. Y. Sung, K. S. Wong, P. Gao, I. D. Williams, H. S. Kwok and B. Z. Tang, *J. Phys. Chem. B*, 2005, **109**, 10061.

28 Y. Dong, J. W. Y. Lam, Z. Li, A. Qin, H. Tong, Y. Dong, X. Feng and B. Z. Tang, *J. Inorg. Organomet. Polym. Mater.*, 2005, **15**, 287.

29 Q. Zeng, Z. Li, Y. Dong, C. Di, A. Qin, Y. Hong, L. Ji, Z. Zhu, C. K. W. Jim, G. Yu, Q. Li, Z. Li, Y. Liu, J. Qin and B. Z. Tang, *Chem. Commun.*, 2007, 70 and references cited therein.

30 (*a*) H. Tong, Y. Hong, Y. Dong, Y. Ren, M. Haeussler, J. W. Y. Lam, K. S. Wong and B. Z. Tang, *J. Phys. Chem. B*, 2007, **111**, 2000; (*b*) H. Tong, Y. Dong, Y. Hong, M. Haeussler, J. W. Y. Lam, H. H. Y. Sung, X. Yu, J. Sun, I. D. Williams, H. S. Kwok and B. Z. Tang, *J. Phys. Chem. C*, 2007, **111**, 2287; (*c*) H. Tong, Y. Hong, Y. Dong, M. Haeussler, Z. Li, J. W. Y. Lam, Y. Dong, H. H. Y. Sung, I. D. Williams and B. Z. Tang, *J. Phys. Chem. B*, 2007, **111**, 11817.

31 (*a*) Y. Dong, J. W. Y. Lam, A. Qin, Z. Li, J. Sun, Y. Dong and B. Z. Tang, *J. Inorg. Organomet. Polym. Mater.*, 2007, **17**, 673; (*b*) Y. Dong, J. W. Y. Lam, A. Qin, J. Sun, J. Liu, Z. Li, J. Sun, H. H. Y. Sung, I. D. Williams, H. S. Kwok and B. Z. Tang, *Chem. Commun.*, 2007, 3255; (*c*) Y. Dong, J. W. Y. Lam, A. Qin, J. Liu, Z. Li, B. Z. Tang, J. Sun and H. S. Kwok, *Appl. Phys. Lett.*, 2007, **91**, 011111; (*d*) H. Tong, Y. Dong, M. Haeussler, J. W. Y. Lam, H. H. Y. Sung, I. D. Williams, J. Sun and B. Z. Tang, *Chem. Commun.*, 2006, 1133.

32 Y. Dong, J. W. Y. Lam, A. Qin, Z. Li, J. Sun, H. H. Y. Sung, I. D. Williams and B. Z. Tang, *Chem. Commun.*, 2007, 40.

33 (*a*) C. M. O'Donnell and J. D. Winefordner, *Clin. Chem. (Washington, D. C.)*, 1975, **21**, 285; (*b*) R. Snyder and A. C. Testa, *J. Phys. Chem.*, 1978, **82**, 842; (*c*) Y. Nagano, T. Ikoma, K. Akiyama and S. Tero-Kubota, *Chem. Phys. Lett.*, 1999, **303**, 201; (*d*) M. Wahadoszamen, T. Hamada, T. Iimori, T. Nakabayashi and N. Ohta, *J. Phys. Chem. A*, 2007, **111**, 9544.

34 (*a*) W. Rettig, *Angew. Chem., Int. Ed. Engl.*, 1986, **25**, 971; (*b*) K. Bhattacharyya and M. Chowdhury, *Chem. Rev.*, 1993, **93**, 507; (*c*) R. S. Davidson, *Chem. Soc. Rev.*, 1996, **25**, 241; (*d*) Z. R. Grabowski, K. Rotkiewicz and W. Rettig, *Chem. Rev.*, 2003, **103**, 3899.

35 H. Tong, Y. Dong, M. Haeussler, Y. Hong, J. W. Y. Lam, H. H. Y. Sung, I. D. Williams, H. S. Kwok and B. Z. Tang, *Chem. Phys. Lett.*, 2006, **428**, 326.

36 E. Lager, J. Z. Liu, A. Aguilar-Aguilar, B. Z. Tang and E. Peña-Cabrera, *J. Org. Chem.*, 2009, **74**, 2053.

37 A. Loudet and K. Burgess, *Chem. Rev.*, 2007, **107**, 4891.

38 (*a*) K. Rurack, M. Kollmannsberger, U. Resch-Genger and J. Daub, *J. Am. Chem. Soc.*, 2000, **122**, 968; (*b*) J. L. Bricks, A. Kovalchuk, C. Trieflinger, M. Nofz, M. Buschel, A. I. Tolmachev, J. Daub and K. Rurack, *J. Am. Chem. Soc.*, 2005, **127**, 13522; (*c*) E. M. Nolan and S. J. Lippard, *J. Am. Chem. Soc.*, 2007, **129**, 5910; (*d*) T. L. Andrew and T. M. Swager, *J. Am. Chem. Soc.*, 2007, **129**, 7254.

39 B. Z. Tang, H. Chen, R. Xu, J. W. Y. Lam, K. K. L. Cheuk and H. N. C. Wong, *Chem. Mater.*, 2000, **12**, 213.

40 Y. Dong, J. W. Y. Lam, A. Qin, Z. Li, J. Liu, J. Sun, Y. Dong and B. Z. Tang, *Chem. Phys. Lett.*, 2007, **446**, 124.

41 Z. Li, Y. Q. Dong, J. W. Y. Lam, J. Sun, A. Qin, M. Häußler, Y. P. Dong, H. H. Y. Sung, I. D. Williams, H. S. Kwok and B. Z. Tang, *Adv. Funct. Mater.*, 2009, **19**, 905.

42 X. Zhang and J. C. Shen, *Adv. Mater.*, 1999, **11**, 1139.

43 (*a*) J. Jin, J. Sun, Y. Dong, H. Xu, W. Yuan and B. Z. Tang, *J. Lumin.*, 2009, **129**, 19; (*b*) L. Tang, J. Jin, S. Zhang, Y. Mao, J. Sun, W. Yuan, H. Zhao, H. Xu, A. Qin and B. Z. Tang, *Sci. China Ser. B: Chem*, 2009, **52**, 755; (*c*) J. Jin, *MS Thesis*, Zhejiang University, May 2008.

44 (*a*) M. Zürcher and F. Diederich, *J. Org. Chem.*, 2008, **73**, 4345; (*b*) M. G. Gold, D. Barford and D. Komander, *Curr. Opin. Struct. Biol.*, 2006, **16**, 693; (*c*) S. Lindskog, *Pharmacol. Ther.*, 1997, **74**, 100.

45 C. P. Y. Chan, M. Haeussler, B. Z. Tang, Y. Dong, K. K. Sin, W. C. Mak, D. Trau, M. Seydack and R. Renneberg, *J. Immunol. Methods*, 2004, **295**, 111.

46 H. Tong, Y. Hong, Y. Dong, M. Haeussler, J. W. Y. Lam, Z. Li, Z. Guo, Z. Guo and B. Z. Tang, *Chem. Commun.*, 2006, 3705.

47 Y. Hong, M. Haeussler, J. W. Y. Lam, Z. Li, K. K. Sin, Y. Dong, H. Tong, J. Liu, A. Qin, R. Renneberg and B. Z. Tang, *Chem.–Eur. J.*, 2008, **14**, 6428.

48 (*a*) *Commercial Biosensors: Applications to Clinical, Bioprocess and Environmental Samples*, ed. G. Ramsay, Wiley, New York, 1998; (*b*) *Fluorescent Chemosensors for Ion and Molecule Recognition*, ed. A. W. Czarnik, ACS, Washington, DC, 1992; (*c*) N. Fujita, S. Shinkai and T. D. James, *Chem.–Asian J.*, 2008, **3**, 1076; (*d*) T. D. James, K. R. A. S. Sandanayake and S. Shinkai, *Angew. Chem., Int. Ed. Engl.*, 1996, **35**, 1910; (*e*) T. D. James, K. R. A. S. Sandanayake and S. Shinkai, *Nature*, 1995, **374**, 345.

49 (*a*) H. Eggert, J. Frederiksen, C. Morin and J. C. Norrild, *J. Org. Chem.*, 1999, **64**, 3846; (*b*) A.-J. Tong, A. Yamauchi, T. Hayashita, Z.-Y. Zhang, B. D. Smith and N. Teramae, *Anal. Chem.*, 2001, **73**, 1530; (*c*) N. DiCesare, M. R. Pinto, K. S. Schanze and J. R. Lakowicz, *Langmuir*, 2002, **18**, 7785.

50 H. Tong, J. W. Y. Lam, M. Häußler, Y. Q. Dong and B. Z. Tang, *Polym. Prepr. (Am. Chem. Soc., Div. Polym. Chem.)*, 2005, **46**(2), 1038.

51 (*a*) G. Springsteen and B. A. Wang, *Tetrahedron*, 2002, **58**, 5291; (*b*) J. C. Norrild and H. Eggert, *J. Am. Chem. Soc.*, 1995, **117**, 1479; (*c*) M. P. Nicholls and P. K. C. Paul, *Org. Biomol. Chem.*, 2004, **2**, 1434.

52 Y. Yu, Y. Hong, C. Feng, J. Liu, J. W. Y. Lam, M. Faisal, K. M. Ng, K. Q. Luo and B. Z. Tang, *Sci. China, Ser. B: Chem.*, 2009, **52**, 15.

53 L. Heng, X. Wang, Y. Dong, J. Zhai, B. Z. Tang, T. Wei and L. Jiang, *Chem.–Asian J.*, 2008, **3**, 1041.

54 L. Feng, S. Li, Y. Li, H. Li, L. Zhang, J. Zhai, Y. Song, B. Liu, L. Jiang and D. Zhu, *Adv. Mater.*, 2002, **14**, 1857.
55 (*a*) L. Heng, J. Zhai, A. Qin, Y. Zhang, Y. Dong, B. Z. Tang and L. Jiang, *ChemPhysChem*, 2007, **8**, 1513; (*b*) K. H. Cheng, Y. Zhong, B. Y. Xie, Y. Q. Dong, Y. Hong, J. Z. Sun, B. Z. Tang and K. S. Wong, *J. Phys. Chem. C*, 2008, **112**, 17507.
56 L. Heng, Y. Dong, J. Zhai, B. Z. Tang and L. Jiang, *Langmuir*, 2008, **24**, 2157.
57 (*a*) J. Chen, Z. Xie, J. W. Y. Lam, C. C. W. Law and B. Z. Tang, *Macromolecules*, 2003, **36**, 1108; (*b*) H. Chen, J. Chen, C. Qiu, B. Z. Tang, M. Wong and H. S. Kwok, *IEEE J. Sel. Top. Quantum Electron.*, 2004, **10**, 10; (*c*) J. Chen, B. Xu, K. Yang, Y. Cao, H. H. Y. Sung, I. D. Williams and B. Z. Tang, *J. Phys. Chem. B*, 2005, **109**, 17086; (*d*) J. Chen, H. S. Kwok and B. Z. Tang, *J. Polym. Sci., Part A: Polym. Chem.*, 2006, **44**, 2487.
58 Abbreviations used to denote the OLED device: ITO = indium tin oxide, CuPc = copper phthalocyanine, and TPD = *N*,*N*′-diphenyl-*N*,*N*′-bis(3-methylphenyl)-1,1′-diphenyl-4,4′-diamine.
59 H. Y. Chen, W. Y. Lam, J. D. Luo, Y. L. Ho, B. Z. Tang, D. B. Zhu, M. Wong and H. S. Kwok, *Appl. Phys. Lett.*, 2002, **81**, 574.
60 E. W. Debler, G. F. Kaufmann, M. M. Meijler, A. Heine, J. M. Mee, G. Pljevaljcic, A. J. Di Bilio, P. G. Schultz, D. P. Millar, K. D. Janda, I. A. Wilson, H. B. Gray and R. A. Lerner, *Science*, 2008, **319**, 1232.
61 J. Dong, K. M. Solntsev and L. M. Tolbert, *J. Am. Chem. Soc.*, 2009, **131**, 662.
62 Some examples of recent work in the area: (*a*) T. Sanji, K. Shiraishi and M. Tanaka, *ACS Appl. Mater. Interfaces*, 2009, **1**, 270; (*b*) S. C. Dong, Z. Li and J. G. Qin, *J. Phys. Chem. B*, 2009, **113**, 434; (*c*) J. Xu, L. Wen, W. Zhou, J. Lv, Y. Guo, M. Zhu, H. Liu, Y. Li and L. Jiang, *J. Phys. Chem. C*, 2009, **113**, 5924; (*d*) M.-X. Zhu, W. Lu, N. Zhu and C.-M. Che, *Chem.–Eur. J.*, 2008, **14**, 9736; (*e*) M. Wang, D. Zhang, G. Zhang and D. Zhu, *Chem. Commun.*, 2008, 4469; (*f*) Y. Zhao, H. Fu, A. Peng, Y. Ma, D. Xiao and J. Yao, *Adv. Mater.*, 2008, **20**, 2859; (*g*) J. W. Chung, B.-K. An, J. W. Kim, J.-J. Kim and S. Y. Park, *Chem. Commun.*, 2008, 2998; (*h*) J. Xu, X. Liu, J. Lv, M. Zhu, C. Huang, W. Zhou, X. Yin, H. Liu, Y. Li and H. Ye, *Langmuir*, 2008, **24**, 4231; (*i*) C.-X. Yuan, X.-T. Tao, Y. Ren, Y. Li, J.-X. Yang, W.-T. Yu, L. Wang and M.-H. Jiang, *J. Phys. Chem. C*, 2007, **111**, 12811; (*j*) J. L. Mullin, H. J. Tracy, J. R. Ford, S. R. Keenan and F. Fridman, *J. Inorg. Organomet. Polym. Mater.*, 2007, **17**, 201; (*k*) S. Kim, Q. Zheng, G. He, D. J. Bharali, H. E. Pudavar, A. Baev and P. N. Prasad, *Adv. Funct. Mater.*, 2006, **16**, 2317; (*l*) R. Davis and S. Das, *J. Fluoresc.*, 2005, **15**, 749; (*m*) M. Han and M. Hara, *J. Am. Chem. Soc.*, 2005, **127**, 10951; (*n*) K. Itami, Y. Ohashi and J. Yoshida, *J. Org. Chem.*, 2005, **70**, 2778; (*o*) S. H. Lee, B. B. Jang and Z. H. Kafafi, *J. Am. Chem. Soc.*, 2005, **127**, 9071; (*p*) T. Mutai, H. Satou and K. Araki, *Nat. Mater.*, 2005, **4**, 685; (*q*) M. Shimizu, Y. Takeda, M. Higashi and T. Hiyama, *Angew. Chem., Int. Ed.*, 2009, **48**, 3653; (*r*) H. Yu and L. Qi, *Langmuir*, 2009, DOI: 10.1021/la900296y; (*s*) Y. Chen, Y. Lv, Y. Han, B. Zhu, F. Zhang, Z. Bo and C.-Y. Liu, *Langmuir*, 2009, DOI: 10.1021/la803436h.